Dynamic Correlations in a Classical Two-dimensional Heisenberg Antiferromagnet

G. M. Wysin
Department of Physics, Cardwell Hall,
Kansas State University, Manhattan, KS 66506-2601
and
A. R. Bishop
Theoretical Division and Center for Nonlinear Studies
Los Alamos National Laboratory, Los Alamos, NM 87545

Abstract

A Monte Carlo–molecular dynamics calculation of the dynamic structure function $S(\mathbf{q},\omega)$ for the classical two-dimensional isotropic Heisenberg antiferromagnet is presented. For wavevectors near the antiferromagnetic Bragg point, $S(\mathbf{q},\omega)$ is well-described by a product of Lorentzians representing damped spin waves. For adequately low temperatures, the dependence of the spin wave frequency and damping on wavevector and temperature are consistent with a dynamic scaling description of Chakravarty, Halperin and Nelson. Even for higher temperatures a scaling description is quite well satisfied, but with a modified scaling frequency.

Phys. Rev. B 42, 810 (1990).

I. Introduction

Studies of spin dynamics in quasi-2-dimensional materials have received a significant boost in the last several years because of the convergence of: (a) improved quasi-2-dimensional magnetic materials; (b) low-frequency, long-wavelength inelastic neutron scattering data; and (c) simulation capabilities for large sized lattices. Materials with various spin symmetries have been studied, probing vortex, domain wall and spin wave dynamics and interactions.[1]

In this context, the copper oxide based high-temperature superconductors in their undoped (antiferromagnetic, non-superconducting) phase are now appreciated to be excellent examples of very 2-dimensional, antiferromagnetic, near-isotropic Heisenberg Hamiltonians.[2] This antiferromagnetism has been probed[2] by preliminary inelastic neutron scattering, NMR, etc. Comparisons with theory of the 2-D isotropic Heisenberg model are very successful, except for a small Dzyaloshinsky-Moriya term appearing in the real materials. This experimental-theoretical agreement is particularly well-confirmed for static spin correlations which are very long ranged, even at substantial temperatures. For dynamics, the data is much less complete at present, and theory[3] has emphasized a dynamic scaling expectation and its consequences. The real materials are extremely quantum (S=1/2) and the theory procedes by mapping the quantum isotropic Heisenberg Hamiltonian to a quantum O(3) nonlinear sigma model, whose scaling properties are studied by including quantum fluctuations into a classical O(3) model. Furthermore, the O(3) model can be mapped to a ferromagnetic rotor model at sufficiently low frequencies and long wavelengths, and this latter classical model has been studied numerically in a Langevin molecular dynamics (MD) simulation,[4] described below. This simulation appears to support the analytic dynamic scaling expectations. An alternative analytic procedure has been suggested by Reiter,[5] who used a low-T and (1/S) perturbative memory function approach for dynamic correlation functions. It is not clear whether this approach yields subtle violations of dynamic scaling, without further explicit evaluations.

It is of interest to explore the dynamics of the antiferromagnetic Heisenberg model directly in order to confirm the scaling behavior, to extend expectations (which can be

compared with experiment) outside the scaling regime, and to incorporate additional symmetry-breaking terms, inter-plane coupling, etc. The most complete approach is quantum Monte Carlo. This has been implemented for static properties,[6,7] and extracting frequency dependence from the imaginary time simulation data is probably also practical within some reasonable restrictions on the form of the dynamic structure function. Our aim in this paper is more limited. Namely, we wish to implement a classical ($S = \infty$) MD simulation to test dynamic scaling, and to establish a form for the scaling function and observe deviations at higher T, in the original discrete antiferromagnetic isotropic Heisenberg model. This avoids mapping to O(3) sigma or rotor models.

As mentioned above, Chakravarty, Halperin and Nelson (CHN) have developed a scaling theory[2] for the low temperature dynamic properties of the quantum Heisenberg antiferromagnet in two dimensions (QHAF). For adequately low temperatures, and wavevectors q close to the antiferromagnetic Bragg point, CHN have suggested that the dynamic properties of the QHAF can be obtained from dynamic properties of a *classical* lattice rotor model (CLRM). The CHN theory is a *dynamic scaling* theory, in the sense that dynamic properties, such as spin-wave frequencies, when measured at different temperatures, can be related to each other easily, provided that frequencies and wavelengths are appropriately re-scaled. The physical length scale at any temperature T is the spin-spin correlation length $\xi(T)$, which is the factor for re-scaling wavevectors.

For dynamics, the theory requires a temperature-dependent physical time scale $\tau_s(T)$, or alternatively a scaling frequency $\omega_s(T) = 2\pi/\tau_s$. The time-scale τ_s is the re-scaling factor for frequencies, and is closely related to the *damping rate* or linewidth for the spinwaves. The scaling assumption asserts that the frequency and wavevector dependencies of dynamic quantities will be determined only by the dimensionless re-scaled variables, $\mathbf{Q} = \mathbf{q}\xi$, and $\Omega = \omega\tau_s$, rather than by ω, q, and T separately. Through the use of a renormalization group (RG) analysis, CHN give specific expressions for the temperature dependence of the correlation length ξ and time τ_s.

To test the CHN theory, Tyc, Halperin, and Chakravarty (THC) have recently reported results[4] of a Langevin dynamics simulation of a classical lattice rotor model,

wherein the dynamic structure function, $S(\mathbf{q},\omega)$, was calculated numerically using a large lattice (256×256). For some set of wavevectors and temperatures satisfying the assumptions of the CHN theory, they obtained a reasonable fit to the scaling theory, by adjusting several parameters describing the scaling functions for spinwave frequency and damping rate.

It is our purpose here to report results of a related simulation, directly for the 2D *classical* Heisenberg antiferromagnet, which also substantially supports the dynamic scaling hypothesis. The classical isotropic spin model under consideration is

$$H = J \sum_{(\mathbf{n},\mathbf{m})} \vec{\mathbf{S}}_{\mathbf{n}} \cdot \vec{\mathbf{S}}_{\mathbf{m}} \tag{1.1}$$

where $J > 0$ is the exchange constant, $\vec{\mathbf{S}}_{\mathbf{n}}$ is a classical (three-component) spin vector at a lattice site $\mathbf{n}$ on a square lattice, and the sum is only over nearest neighbor pairs. Note that we use the symbol $\mathbf{q} = (1,1)\pi/a - \mathbf{k}$ to denote wavevectors measured from the antiferromagnetic Bragg point, $(1,1)\pi/a$. The lattice constant is a.

The principal quantity calculated in these simulations is the dynamic correlation function, $S(\mathbf{q},\omega)$, which is the space-time Fourier transform of the space and time displaced correlation function (see below). By fitting $S(\mathbf{q},\omega)$ to an assumed Lorentzian response function, the spin-wave frequency $\omega_{\mathbf{q}}$ and damping rate $\gamma_{\mathbf{q}}$ were determined numerically, and found to follow scaling relationships similar to those given by CHN. The scaling frequency $\omega_s(T)$ we obtained is consistent with the CHN theory except for temperatures greater than $T \approx 0.80$, which are probably outside of the scaling regime.

Our simulation differs from that of THC principally in three respects: i) THC have simulated a classical rotor model, with a Hamiltonian that includes a kinetic energy term in addition to a *ferromagnetic* nearest neighbor interaction. Of course, that choice was based on the CHN mapping to the QHAF mentioned above; to obtain properties of the $S = 1/2$ QHAF. Our simulation represents the opposite limit, $S \to \infty$; ii) By employing a Langevin type of equation to simulate finite temperatures, THC made use of the canonical ensemble, by coupling to a heat bath via random forces with a prescribed correlation, together with a small phenomenological damping. On the other hand, we have used a two-step simulation, using a (canonical ensemble) Monte Carlo

(MC) algorithm to produce states for a desired temperature, which were subsequently used as initial states for an energy-conserving spin-dynamics (MD) integration of the classical equations of motion, in a microcanonical ensemble. iii) We have used a 100 $\times$ 100 lattice ($L = 100$), smaller than that used by THC by a factor of 0.40 ($L = 256$). The lowest accessible temperature is determined roughly by the point at which the correlation length equals half the lattice size. The RG analysis and numerical results give $\xi \approx 130a$ at $T/JS^2 = 0.52$, and $\xi \approx 50a$ at $T/JS^2 = 0.57$, so the THC calculation is valid to only *slightly* lower temperatures than results presented here. The lowest accesible wavevector (either measured from $(0,0)\pi/a$ or from $(1,1)\pi/a$) is $q = 2\pi/La$, so that the major advantage of using a larger system size is access to much smaller wavevectors.

We begin in Sec. II by summarizing some general properties of the 2D Heisenberg antiferromagnet, within the scaling hypothesis. This includes a low precision fit to determine the correlation length for our finite system, followed by a description of the scaling hypothesis and scaling functions. In Sec. III and IV we will describe the details of the numerical simulation, along with a discussion of the fitting functions used for describing the spin-wave frequency and linewidths. We then present two methods in Sec. V for obtaining rough estimates of the scaling frequency $\omega_s(T)$, and from those obtain refined estimates. In the process of estimating $\omega_s(T)$, we graphically obtain scaling functions for spin-wave frequency and linewidth. Sec. VI contains concluding remarks.

II. Scaling in the Classical Heisenberg Antiferromagnet

A principal interest here is to describe the dynamic signature of the spinwaves in a 2D system. Of course, the lack of long range order at finite temperature, as given by the Mermin-Wagner theorem,[8] needs to be recognized. However, there *is* short range order, on length scales less than the correlation length. Therefore, the modification from 3D spinwave theory is that the spinwaves represent local perturbations from short range order, and can be used as well-defined modes as long as their wavelengths are much shorter than the correlation length(i.e., $q\xi >> 1$). In addition, the interactions among an equilibrium population of these modes at finite temperature leads to a damping of

the modes. This gives a mode at any wavevector q a finite lifetime, or equivalently, a nonzero frequency width $\gamma_{\mathbf{q}}$, about the center frequency, $\omega_{\mathbf{q}}$. For some range of wavevectors and temperatures, we are interested in finding $\gamma_{\mathbf{q}}$ and $\omega_{\mathbf{q}}$. For comparison, Tyč and Halperin,[9] and Becher and Reiter[10], have each given leading order perturbation expansions to obtain $\gamma_{\mathbf{q}}$ and $\omega_{\mathbf{q}}$, with somewhat different results, especially for the temperature dependence of $\gamma_{\mathbf{q}}$.

To determine the wavevector range where perturbation expansions will be applicable, we can make some estimates of the correlation length, and compare with other work. Shenker and Tobochnik[11] (SB) have determined the correlation length using a MC RG technique. Also, CHN have given an expression for the static structure function,

$$S(\mathbf{q}) = \frac{1}{3} < \vec{S}_{\mathbf{q}} \cdot \vec{S}_{-\mathbf{q}} > \tag{2.1}$$

where

$$\vec{S}_{\mathbf{q}} = \frac{1}{N} \sum_{\mathbf{n}} e^{i\mathbf{q}\cdot\mathbf{r}_{\mathbf{n}}} \vec{S}_{\mathbf{n}} \tag{2.2}$$

are the spatial Fourier modes, with N the number of spins in the system. The CHN RG analysis gives a modified Ornstein-Zernicke form (OZ),

$$S(\mathbf{q}) = S(q=0) \frac{1 + \frac{1}{2} B_f \ln[1 + (q\xi)^2]}{1 + (q\xi)^2}. \tag{2.3}$$

THC found $B_f \approx 4\pi/125$. The effect of the logarithm term is greatest at low temperature. If we take this expression to be valid, but restrict to small wavevectors, $q\xi \leq 1$, then the effect of the logarithm is negligible and the q-dependence is very closely of the OZ form. Then we can extract estimates of the correlation length from OZ plots as in Figure 1. The curves of $S(q=0)/S(q) - 1$ vs. q^2 for various temperatures have slopes that are the squares of the correlation length for that temperature. These data were produced from the MC calculation described below. Over the range of q shown, for temperatures $0.55 \leq T \leq 1.0$, the OZ form is fairly closely followed. We did not look carefully for the logarithmic corrections indicated above. The resulting correlation lengths are shown in Figure 2, and compared with the low temperature RG result of CHN,

$$\xi(T) = B_\xi a \frac{\exp(2\pi J S^2/T)}{1 + 2\pi J S^2/T}. \tag{2.4}$$

Here $B_\xi \approx 0.01$ is a fitting parameter that was obtained by Shenker and Tobochnik.[11] For lower temperatures, $T < 0.65$, the effects of the finite sized lattice clearly limit the correlation length. For temperatures greater than $T \approx 0.8$, our data also deviate from the low temperature RG prediction, but are consistent with the SB results and high temperature series.

For dynamic correlations, consider the temporal Fourier transform of the time-displaced correlation function,

$$S(\mathbf{q},\omega) = \frac{1}{2\pi}\int_{-\infty}^{\infty} dt\; e^{-i\omega t}\frac{1}{3} < S_{\mathbf{q}}(0)\cdot S_{-\mathbf{q}}(t) > . \tag{2.5}$$

According to the scaling theory of CHN, this dynamic structure function can be written in the scaled form,[2]

$$S(\mathbf{q},\omega) = \omega_s^{-1} S(q)\Phi(\mathbf{Q},\Omega), \tag{2.6}$$

where $\omega_s(T)$ is the temperature-dependent frequency scale ($= 2\pi/\tau_s$), and Φ is a dimensionless scaling function, of the scaled variables,

$$\mathbf{Q} \equiv \mathbf{q}\xi, \qquad \Omega \equiv \omega/\omega_s. \tag{2.7}$$

Note that $S(q)$ is actually assumed to be a function of $q\xi$ and T, by equation (2.3) above (but *not* of q itself). Then one can see that the essential feature of the scaling assumption is that the wavevector and frequency dependencies of $S(\mathbf{q},\omega)$ are assumed to be determined only by the scaled variables Q and Ω, independent of the temperature. The only effect of the temperature is a re-scaling of the magnitude of $S(\mathbf{q},\omega)$. CHN give the following expression for the frequency scale:

$$\omega_s = c\xi^{-1}(T/2\pi JS^2)^{1/2}, \tag{2.8}$$

with $c = \sqrt{8}JS^2a/\hbar$ being the zero temperature long wavelength spinwave velocity. In analyzing $S(\mathbf{q},\omega)$ data, we take $\omega_s(T)$ to be a freely adjustable function, determined via least squares curve fits to $S(\mathbf{q},\omega)$, as described below. The scaling function $\Phi(\mathbf{Q},\Omega)$ is also an unknown function, not prescribed by scaling theory, to be determined by the fits. However, this is intractable unless some simple functional form for Φ is assumed, possessing a limited number of fitting parameters.

This, to determine Φ, the data for $S(\mathbf{q},\omega)$ is to be fit to an assumed functional form, the simplest of which represents the frequency response of a damped harmonic oscillator. As one of the simplest possible choices for $\Phi(\mathbf{Q},\Omega)$, THC have used a sum of two Lorentzians, with equal widths but centered at opposite frequencies. However, when they compared their least squares curve fits with their original MD data for $S(\mathbf{q},\omega)$, at fixed $\mathbf{q}$, it was clear that the fitted curves fell below the data at low frequencies ($\omega < \omega_{\mathbf{q}}$), and fell consistently above the data at higher frequencies ($\omega > \omega_{\mathbf{q}}$). Our curve fits to a sum of Lorentzians for $S(\mathbf{q},\omega)$ also consistently give the same "anomolous" behavior for the temperatures presented here. This is apparently a consequence of the isotropic symmetry of the Heisenberg Hamiltonian, which places some restrictions on allowed forms for $S(\mathbf{q},\omega)$. To be specific, $\dot{S}(\mathbf{q},t \rightarrow 0)$ *must be zero.* This restriction can be shown to rule out a sum of Lorentzians as a choice for Φ; an alternative which dose not violate this requirement is a *product* of Lorentzians, and is shown below to be a natural choice.

We can demonstrate this restriction on $S(\mathbf{q},\omega)$ using the equations of motion as follows. The classical equations of motion resulting from Hamiltonian (1.1) are

$$\frac{d\vec{\mathbf{S}}_{\mathbf{n}}}{dt} = \vec{\mathbf{S}}_{\mathbf{n}} \times \vec{\mathbf{F}}_{\mathbf{n}}, \tag{2.9}$$

$$\vec{\mathbf{F}}_{\mathbf{n}} = -J \sum_{(\mathbf{n},\mathbf{m})} \vec{\mathbf{S}}_{\mathbf{m}}, \tag{2.10}$$

where $\vec{\mathbf{F}}_{\mathbf{n}}$ is the effective field acting on $\vec{\mathbf{S}}_{\mathbf{n}}$ produced by all of its nearest neighbors; the sum in Eqn. (2.10) is only over the nearest neighbors of $\mathbf{n}$.

Using the spatial Fourier modes defined above in equation (2.2), one component of the time-displaced correlation function can be written as

$$S^{\alpha\alpha}(\mathbf{q},t) = \frac{1}{N^2} \sum_{\mathbf{n},\mathbf{m}} e^{i\mathbf{q}\cdot(\mathbf{r_n}-\mathbf{r_m})} < S^{\alpha}_{\mathbf{n}}(0) S^{\alpha}_{\mathbf{m}}(t) > . \tag{2.11}$$

The $t = 0$ time derivative of this is

$$\dot{S}^{\alpha\alpha}(\mathbf{q},0) = < S^{\alpha}_{\mathbf{q}}(0) \dot{S}^{\alpha}_{-\mathbf{q}}(0) > = \frac{1}{N^2} \sum_{\mathbf{n},\mathbf{m}} e^{i\mathbf{q}\cdot(\mathbf{r_n}-\mathbf{r_m})} < S^{\alpha}_{\mathbf{n}}(0) \dot{S}^{\alpha}_{\mathbf{m}}(0) > . \tag{2.12}$$

This can be evaluated in terms of the equal-time averages, $< S^{\alpha}_{\mathbf{n}}(0)\dot{S}^{\alpha}_{\mathbf{m}}(0) >$, which are equilibrium averages that are readily evaluated. For example, consider $\alpha = x$, with equation of motion for this component

$$\dot{S}^{x}_{\mathbf{m}} = -J \sum_{(\mathbf{m},\mathbf{m}')} (S^{y}_{\mathbf{m}} S^{z}_{\mathbf{m}'} - S^{z}_{\mathbf{m}} S^{y}_{\mathbf{m}'}). \tag{2.13}$$

The sum is over the neighbors $\mathbf{m}'$ of site $\mathbf{m}$. This is multiplied by $S^{x}_{\mathbf{n}}$ and then the equilibrium expectation value is taken:

$$< S^{x}_{\mathbf{n}} \dot{S}^{x}_{\mathbf{m}} >= -J \sum_{(\mathbf{m},\mathbf{m}')} (< S^{x}_{\mathbf{n}} S^{y}_{\mathbf{m}} S^{z}_{\mathbf{m}'} > - < S^{x}_{\mathbf{n}} S^{z}_{\mathbf{m}} S^{y}_{\mathbf{m}'} >). \tag{2.14}$$

However, the isotropic Hamiltonian is invariant under a re-labeling of the y and z spin axes, so that $< S^{x}_{\mathbf{n}} S^{y}_{\mathbf{m}} S^{z}_{\mathbf{m}'} >=< S^{x}_{\mathbf{n}} S^{z}_{\mathbf{m}} S^{y}_{\mathbf{m}'} >$. Then in this case the two terms in Eq. (2.14) are identical and cancel, regardless of whether $\mathbf{n} = \mathbf{m}$, or whether $\mathbf{n}$ is a neighbor of $\mathbf{m}$ or not. Thus we conclude that for the Heisenberg model,

$$< S^{z}_{\mathbf{n}} \dot{S}^{z}_{\mathbf{m}} >=< S^{y}_{\mathbf{n}} \dot{S}^{y}_{\mathbf{m}} >=< S^{x}_{\mathbf{n}} \dot{S}^{z}_{\mathbf{m}} >= 0, \tag{2.15}$$

for *any* sites $\mathbf{n}$ and $\mathbf{m}$. For $\mathbf{n} = \mathbf{m}$ this is just a statement of the conserved spin length. However, since the isotropic symmetry makes it true more generally, then we also have

$$< S^{\alpha}_{\mathbf{q}}(0) \dot{S}^{\alpha}_{-\mathbf{q}}(0) >= 0, \tag{2.16}$$

for $\alpha = x, y$, or z (which are all equal). In similar fashion, for an XY-model, the invariance of the Hamiltonian with respect to re-labeling x and y spin axes, implies only that $< S^{z}_{\mathbf{q}}(0) \dot{S}^{z}_{-\mathbf{q}}(0) >$ is zero.

An apropriate form for $S(\mathbf{q}, t)$, consistent with the above restriction, is

$$S(\mathbf{q}, t) = A e^{-\gamma_{\mathbf{q}}|t|} \{\cos \omega_{\mathbf{q}} t + \frac{\gamma_{\mathbf{q}}}{\omega_{\mathbf{q}}} \mathrm{sign}(t) \sin \omega_{\mathbf{q}} t\}. \tag{2.17}$$

The parameters $\omega_{\mathbf{q}}$ and $\gamma_{\mathbf{q}}$ are to be fit as functions of $\mathbf{q}$ and T. This function is the response of an underdamped harmonic oscillator that starts with zero velocity from some initial displacement A, and is constructed to be an even real function of t. The

initial displacement A is identified as $S(\mathbf{q}, t = 0)$. The two-sided Fourier transform is also real;

$$S(\mathbf{q},\omega) = \frac{1}{2\pi}\int_{-\infty}^{+\infty} dt\ S(\mathbf{q},t)e^{-i\omega t} = \frac{2A\gamma_\mathbf{q}(\gamma_\mathbf{q}^2+\omega_\mathbf{q}^2)/\pi}{[(\omega+\omega_\mathbf{q})^2+\gamma_\mathbf{q}^2][(\omega-\omega_\mathbf{q})^2+\gamma_\mathbf{q}^2]}, \tag{2.18}$$

and is a *product* of two symmetrically located Lorentzians.[12]

Alternatively, note that if a *sum* of symmetrically located Lorentzians is assumed for $S(\mathbf{q},\omega)$, i. e.

$$S(\mathbf{q},\omega) = \frac{A\gamma_\mathbf{q}}{2\pi}\{\frac{1}{(\omega+\omega_\mathbf{q})^2+\gamma_\mathbf{q}^2} + \frac{1}{(\omega-\omega)_\mathbf{q}^2+\gamma_\mathbf{q}^2}\}, \tag{2.19}$$

then the time-correlation is

$$S(\mathbf{q},t) = Ae^{-\gamma_\mathbf{q}|t|}\cos\omega_\mathbf{q}t. \tag{2.20}$$

This function has a discontinuous non-zero time derivative at $t = 0$; $\dot{S}(\mathbf{q},0^+) = -A\gamma_\mathbf{q}$, and $\dot{S}(\mathbf{q},0^-) = +A\gamma_\mathbf{q}$, and making it unsuitable for use in the present context, especially for strong damping, at short times (high frequencies).

There is also the possibility of fitting to the response of an *overdamped* harmonic oscillator, which may be relevant especially for higher temperatures. Then we would have a non-oscillatory time dependence,

$$S(\mathbf{q},t) = Ae^{-\gamma_\mathbf{q}|t|}\{\cosh\omega_\mathbf{q}t + \frac{\gamma_\mathbf{q}}{\omega_\mathbf{q}}\mathrm{sign}(t)\sinh\omega_\mathbf{q}t\}. \tag{2.21}$$

In this case the Fourier transform is also a product of Lorentzians, each centered at zero frequency, but having different widths:

$$S(\mathbf{q},\omega) = \frac{2A\gamma_\mathbf{q}(\gamma_\mathbf{q}^2-\omega_\mathbf{q}^2)/\pi}{[\omega^2+(\gamma_\mathbf{q}+\omega_\mathbf{q})^2][\omega^2+(\gamma_\mathbf{q}-\omega_\mathbf{q})^2]}\quad , \tag{2.22}$$

Generally, however, it was not possible to describe the behavior of $S(\mathbf{q},t)$ by these overdamped functions; in all cases discussed here the response of $S(\mathbf{q},t)$ involved oscillatory behavior, and was quite well described by the underdamped oscillator formulas, even for higher temperatures and $\mathbf{q}$ near $(1,1)\pi/a$.

To complete the scaling description, note that Eq. (2.18) has exactly the scaling form of Eq. (2.6), provided that the spinwave frequency and damping can be written in terms of undetermined, dimensionless scaled functions $\Omega(\mathbf{q}\xi)$ and $\Gamma(\mathbf{q}\xi)$:

$$\omega_{\mathbf{q}}(T) = \omega_s(T)\Omega(\mathbf{q}\xi), \tag{2.23}$$

$$\gamma_{\mathbf{q}}(T) = \omega_s(T)\Gamma(\mathbf{q}\xi). \tag{2.24}$$

All of the explicit temperature dependence of $\omega_{\mathbf{q}}$ and $\gamma_{\mathbf{q}}$ is given through the ω_s dependence. Then the assumed form of $\Phi(\mathbf{Q},\Omega)$ is (with $\mathbf{Q} = \mathbf{q}\xi$)

$$\Phi(\mathbf{Q},\Omega) = \frac{2\Gamma_{\mathbf{Q}}(\Gamma_{\mathbf{Q}}^2 + \Omega_{\mathbf{Q}}^2)/\pi}{[(\Omega+\Omega_{\mathbf{Q}})^2 + \Gamma_{\mathbf{Q}}^2][(\Omega-\Omega_{\mathbf{Q}})^2 + \Gamma_{\mathbf{Q}}^2]}. \tag{2.25}$$

This function is normalized such that

$$\int_{-\infty}^{+\infty} d\Omega\ \Phi(\mathbf{Q},\Omega) = 1, \tag{2.26}$$

and

$$\Phi(0,0) = \frac{2}{\pi\Gamma_0}, \tag{2.27}$$

with the assumption $\Omega_0 = 0$. It is interesting to note that Eq. (2.27) also would hold had we assumed a single Lorentzian for $\mathbf{Q} = 0$.

Equation (2.24) gives a direct method of estimating *relative* values of ω_s from MD data. The $q = 0$ spinwave linewidth directly gives $\omega_s\Gamma_0$. Of course this method requires first making the fit to obtain $\gamma_{\mathbf{q}}$. An alternative procedure is to make use of the $q = 0, \omega = 0$ datum, for which the scaling assumptions (2.6) and (2.27) above imply

$$\Gamma_0\omega_s = \frac{2}{\pi}\frac{S(0,t=0)}{S(0,\omega=0)}. \tag{2.28}$$

The advantage of this formula is that a fit is not required, although there is still an implicit assumption about the form of $\Phi(\mathbf{Q},\Omega)$ (as in Eq. (2.25)). However, Eq. (2.28) has a fairly intuitive interpretation, especially in terms of the time scale τ_s that results from it. Eq. (2.28) gives

$$\tau_s = \frac{\pi\Gamma_0}{2}\frac{1}{S(0,t=0)}\int_{-\infty}^{+\infty} dt\ S(0,t). \tag{2.29}$$

Apart from the numerical factors, τ_s is the ratio of the area under the $S(0,t)$ curve to the initial value $S(0,t=0)$, which is the simplest way to extract a physical time scale from these quantities. We used both of the above methods for estimating $\omega_s\Gamma_0$ from the numerical simulation data, obtaining very similar results. Both of these methods only give the product, $\omega_s\Gamma_0$, and Γ_0 is undetermined by this fitting procedure. For further analysis, we set $\Gamma_0 = 1$.

III. Numerical Simulation

Numerically we have simulated the classical spin dynamics of the isotropic Hamiltonian in equation (1.1). A 100 x 100 square lattice with periodic boundary conditions was used. The product JS^2 sets the energy scale for this model. Therefore, in numerical results presented here, temperatures will be measured in units of JS^2, frequencies are measured in units of $JS/\hbar$, and wavevectors are measured in units of $1/a$, where a is the lattice spacing.

The method of simulation is a combined Monte Carlo – molecular dynamics technique.[13] First a Monte Carlo simulation is used to equilibrate the system (in a canonical ensemble) to a desired temperature T. A standard Metropolis importance sampling scheme is used. The final state of the Monte Carlo calculation is then used as the initial configuration for an energy-conserving spin-dynamics simulation (in a microcanonical ensemble). Desired time-dependent correlation functions are obtained directly from the spin configuration as it evolves in time. The ensemble average of any time-dependent quantity is then obtained by repeating the spin dynamics calculation using additional initial configurations obtained from new Monte Carlo simulations, and averaging results over the separate initial configurations. Data presented here represent averages over 5 initial configurations.

In the Monte Carlo simulation, the initial state is one in which each spin is given a random initial direction (uniformly distributed on a unit sphere). To encourage the system to sample the allowed phase space in an unbiased manner, trial states for individual spins are also chosen randomly in direction, and then the acceptance rate is determined by the temperature. For temperatures higher than about $T/JS^2 > 0.4$ the resulting acceptance rate is greater than 15 % . For equilibration, the temperature is brought

down to T starting from $3T$, exponentially with time over some equilibration interval of approximately 1000 Monte Carlo passes through the lattice. The updating of spins is done simultaneously on odd/even sublattices in a vectorizable fashion. A total of 10,000 Monte Carlo passes through the lattice (where each pass *attempts* to change every spin) is used after the equilibration interval to generate an initial configuration for the spin dynamics simulation, as well as allowing calculation of thermodynamic functions.

In the spin dynamics simulation, the dynamic equations of motion in terms of the Cartesian components are used, as in equations (2.9) and (2.10). We have integrated these equations numerically using a fourth-order fixed time step Runge–Kutta integration scheme, chosen for its stability and simplicity. Conservation of spin length and energy, to about 1 part in 10^5, served as checks of the numerical acuracy. For the 100 x 100 lattice, the smallest accessible wavevector is $qa = 0.02\pi \approx 0.06$, for which the zero-temperature spin wave frequency is $\omega = cq \approx \sqrt{8}\ 0.06 = 0.17$. To be able to access frequencies several times lower than this and resolve the spin wave peak, we integrated out to times as large as $t = 250/JS$.

Data for time-dependent correlation functions was sampled at 512 equally spaced sampling times separated by $\Delta t = mt_s$, where $t_s = 0.04$ is the fundamental time step for the Runge-Kutta algorithm, and m is an integer from 6 to 12. The spatial Fourier transform, $\vec{\mathbf{S}}_{\mathbf{q}}(t)$, of the spin configuration was saved at these times. The total time interval of integration is $t_F = 511mt_s$. The time-displaced correlation ($\alpha = x, y,$ or z)

$$S^{\alpha\alpha}(\mathbf{q},t) = < S^{\alpha}_{\mathbf{q}}(t_0) \cdot S^{\alpha}_{-\mathbf{q}}(t_0 + t) > \tag{3.1}$$

could then be formed, where $<>$ indicates the average over initial times t_0. In this expression, when a time $t_0 + t$ falls outside of the interval over which data was obtained, a periodic boundary condition in time is assumed. In this way, the number of sampled times used to form $S^{\alpha\alpha}(\mathbf{q},t)$ is independent of t, resulting in better statistics at large times. The time displacement t ranges over a symmetric interval from $-t_F/2$ to $+t_F/2$. With this construction $S^{\alpha\alpha}(\mathbf{q},t)$ is an even function of time. $S^{\alpha\alpha}(\mathbf{q},t)$ was then multiplied by a Gaussian smoothing window function before using a fast Fourier transform to generate the dynamic structure function $S^{\alpha\alpha}(\mathbf{q},\omega)$. The results obtained for $S^{\alpha\alpha}(\mathbf{q},\omega)$

were averaged over 5 initial configurations from the Monte Carlo simulation, and also averaged over the xyz spin components.

IV. Numerical Data and Least Square Fits

Numerical simulations as described above were performed for temperatures in the range $0.1 \leq T/JS^2 \leq 1.0$, for a 100 x 100 lattice. At the lowest temperatures the correlation length was vastly greater than the system size, and we used those points only to check the spinwave frequencies. Equation (2.18) was used for a least-squares fitting of $S(\mathbf{q},\omega)$, for sets of wavevectors covering the entire Brilluion zone along the (11) direction. The parameters $\omega_{\mathbf{q}}$ and $\gamma_{\mathbf{q}}$, and an amplitude in Eq. (2.18) were determined as functions of $\mathbf{q}$ and T.

Some of the data and resulting fitted curves are shown in Figure 3, for $\mathbf{q} = (0.1, 0.1)\pi/a$, and in Figure 4, for $\mathbf{q} = (0.1, 0.1)\pi/a$. The dotted curves are fits to a product of Lorentzians (Eq. (2.18)), and the dashed curves are fits to a sum of Lorentzians (Eq. (2.19)), for comparison. In nearly all cases, the Lorentzian sum passes above the data at higher frequencies and below the data at lower frequencies, while the Lorentzian product follows the data quite well in both frequency ranges. The softening of the spinwave peak with increasing temperature is clear, and is accompanied by an increase in linewidth and decrease in total integrated intensity. At the higher temperatures ($T > 0.80$) the spinwave frequency and linewidth are comparable in size, and it is difficult to distinguish the spinwave frequency by eye. Due to the rather high degree of noise in these data, our estimates of spinwave frequencies are accurate to about 5–10 % (with the frequency grid spacing $\Delta\omega \approx 0.025$). Our estimates of spinwave linewidths are accurate to about 15–20 % .

For the particular case, $q = 0$, with $\omega_q = 0$, we can check whether the $S(\mathbf{q},\omega)$ data follows Eq. (2.18), which reduces to

$$S(0,\omega) = \frac{S(0,\omega=0)}{\left[1 + (\omega/\gamma_{q=0})^2\right]^p}. \tag{4.1}$$

For the Lorentzian product, the power $p = 2$. A graph of $\left[S(0,\omega=0)/S(0,\omega)\right]^{1/p}$ vs. ω^2 will be a straight line if this form is valid, where the slope is $\gamma_{q=0}^{-2}$. We found that

such plots give a straight line for $T/JS^2 \geq 0.70$, using $p = 2$. For lower temperatures, it is likely that a power p somewhere between 1 and 2 is necessary. This may also be an indication that a completely different fundamental form for $S(q,\omega)$ (and $\Phi(Q,\Omega)$) is needed. Nevertheless, we take Eqs. (2.18) and (2.25) as reasonable approximations and continue the analysis using them.

The temperature dependence of the spinwave frequency $\omega_{\mathbf{q}}$ for several wavevectors is shown in Fig. 5. We show temperatures well below those where the calculation would be considered valid for static properties. Yet the $T \to 0$ extrapolation of these data is rather close to the zero temperature dispersion,

$$\omega_q = c \sin qa, \qquad c = \sqrt{8} JSa/\hbar, \tag{4.2}$$

for $\mathbf{q}$ along the (11) direction. The wavevectors shown have magnitudes $qa \approx 0.18, 0.44$, and 0.71, which would have $T = 0$ frequencies $\omega_{\mathbf{q}} \approx 0.50$, 1.22 and 1.85, respectively.

The solid curves in Fig. 5 are a comparison with an expression given by THC for the scaled spinwave frequency,[4]

$$\Omega_{\mathbf{Q}} = fQ\left[\delta + \frac{1}{2}\ln(1+Q^2)\right]^{1/2} \tag{4.3}.$$

The constant f is a factor which is $\sqrt{3/2}$ for the quantum case analyzed by THC and 1 for the classical case here. The parameter δ is an adjustable parameter, which was found to be $\delta \approx 1.7$ for the classical lattice rotor model; we have used $\delta = 2.5$ to get a reasonable fit in Fig. 5. Equations (2.4) and (2.8) for the correlation length and frequency scale were used in combination with (4.3) to produce the solid curves.

The wavevector dependence of the spinwave frequency is shown in Fig. 6, for $T = 0.62$ and $T = 0.85$. The solid curves correspond to $\delta = 2.5$ in Eq. (4.2), and $B_\xi = 0.01$ in Eq. (2.4). At higher temperatures it is difficult to consistently fit both the temperature and wavevector dependence of ω_q using Eq. (4.3). This is probably because that equation is a low temperature prediction, rather than a signature of any lack of scaling.

Figure 7 shows the wavevector dependence of the spinwave linewidth $\gamma_{\mathbf{q}}$, for several temperatures. The solid curves are a comparison to the formula of THC;

$$\Gamma_{\mathbf{Q}} = \frac{\gamma_0(1+\mu q^2)^{1/2}}{\left[1 + \frac{\theta}{2}\ln(1+q^2)\right]^{3/2}}, \tag{4.4}$$

where γ_0, μ, and θ are adjustable parameters. For the curves shown, these were set to $\gamma_0 = 1.7$, $\mu = 1.7$, and $\theta = 0.7$. These values are somewhat different from those used by THC for the CLRM ($\gamma_0 = 0.86$, $\mu = 1.4$, and $\theta = 0.08$.) However, there was considerable freedom in choosing these parameters to reasonably fit the data, and the choice shown here is a rough fit by eye, with the parameters chosen to have the curves fit well at the *lower* temperatures. It was difficult to simultaneously fit the data at high temperatures using Eq. 4.4.

The temperature dependence of the linewidth is more dramatic, shown in Fig. 8 for selected wavevectors. For temperatures below $T \approx 0.65$, the widths were smaller than the frequency resolution of this calculation ($\Delta\omega \approx 0.025$). In particular, the $q = 0$ curve is used to estimate the frequency scale $\omega_s(T)$, for temperatures $T \geq 0.65$. It appears that ω_s increases approximately linearly with T. For temperatures greater than $T \approx 0.8$, the linewidth does not rise as fast as the low-T CHN theory predicts. The product, $\omega_s\xi$ would vary as $T^{1/2}$ according to Eq. (2.8); we may have such a behavior for $T < 0.75$, but above this temperature $\omega_s\xi$ decreases with T (See Table 1).

V. Scaling Functions

The initial estimates of ω_s were refined by constructing a scaling plot as in Figure 9, where ω_q/ω_s is shown as a function of $q\xi$, for data obtained at several temperatures $0.62 \leq T \leq 0.85$. The values of ξ and ω_s used to scale the data, using $\Gamma_0 = 1$, are shown below in Table 1. The ω_s values were chosen to cause the dispersion curves at the different temperatures to fall onto the same curve. It was also found necessary to use correlation lengths closer to those for the infinite system size (see Fig. 2) to get the data to scale well. The resulting curve is a graphical construction of the scaling frequency, Ω_Q vs. Q, and is strong evidence for a scaling description, but probably with ω_s varying somewhat differently than Eq. (2.8), for this temperature range. Similarly, by using the *same* parameters to scale the damping rates, Figure 10 was obtained, and represents the scaling function, Γ_Q. Although there is considerable scatter, the data obtained from the different temperatures is still fairly well-described by the same function.

With an adequate set of simulation data, it should also be possible to determine the scaling function $\Phi(\mathbf{Q}, \Omega)$ graphically, by appropriately scaling the original $S(q, \omega)$

data according to Eq. (2.6). With ξ, ω_s and $S(q)$ known, a plot of $\omega_s S(\mathbf{q},\omega)/S(q)$ vs. ω/ω_s, for fixed scaled wavevector, $\mathbf{q}\xi$, gives $\Phi(\mathbf{Q},\Omega)$. The problem with doing this using a simulation on a small system is that the finite spacing of the accessible wavevectors is too large. This makes it difficult to find many cases of data at the same scaled wavevector, unless the calculations are done for many (closely-spaced) temperatures. However, there were a few cases obtained here with approximately equal values of Q, allowing us to make the plots in Figure 11, for several values of Q. With the appropriate scaling in amplitude, wavevector, and frequency, the structure functions for different temperatures are approximately equal. It was found that these curves will not fall onto each other unless they correspond quite closely to the same value of Q, within about 2–4 % , due to the fairly strong dependencies of amplitude and spinwave frequency on Q. Unfortunately, the ratios of correlation lengths at the two temperatures in these examples are the order of 2; it would be especially useful to study a larger range.

VI. Conclusions

We have used an energy-conserving MC-MD simulation to study spin dynamics in the classical 2-dimensional isotropic Heisenberg antiferromagnet on a 100 x 100 square lattice. In particular, we have examined the dynamic structure function $S(\mathbf{q},\omega)$ near the antiferromagnetic Bragg point (zone boundary) and find that this is well-described by a product of Lorentzians. This product form is unlikely to be exact but is clearly superior to a sum and will be a preferred form for comparison with experimental inelastic neutron scattering data.

Although dynamic scaling theory cannot prescribe the functional form of $S(\mathbf{q},\omega)$, it does yield the dependence of the spinwave frequency and damping on wavevector (close to the zone boundary) and temperature (at sufficiently low temperatures). Comparison of our data with such a scaling theory due to Chakravarty, Halperin and Nelson[3] is found to be entirely consistent. Indeed, even for higher temperatures (short correlations) the same scaling description is quite well satisfied, but with a modified temperature dependent scaling frequency. The scaling theory was developed for a continuum O(3) nonlinear sigma model, equivalent to the original Heisenberg model, and previously successfully tested numerically on a classical lattice rotor model.[4] It is therefore interesting that the

same dynamic scaling theory is indeed valid (within our numerical accuracy) for the original, discrete antiferromagnetic spin model with Landau dynamics.

In the context of high-temperature superconductors or other strongly quantum magnets, numerical progress beyond the present classical level will be possible using quantum MC simulations and extracting real time evolution from that in imaginary time. Such results could directly test approximate quantum extensions of classical results which have been proposed.[10,14,15] As in one-dimensional magnets, the major quantum effect is to reduce the effective magnetic moment and therefore suppress specific heat or integrated scattering intensities. However, more qualitative quantum effects may occur in the frequency dependence itself.

Acknowledgements

Extensive discussions with G. Reiter are gratefully acknowledged. Work at Los Alamos supported by United States Department of Energy.

T	ξ	ω_s	$\omega_s\xi$
0.62	25	0.066	1.65
0.65	14	0.12	1.68
0.70	7.7	0.22	1.69
0.75	5.1	0.34	1.73
0.85	2.8	0.55	1.54

Table 1. Scaling Parameters, with $\Gamma_0 = 1$.

References

[1] For example, F. G. Mertens, A. R. Bishop, G. M. Wysin and C. Kawabata, Phys. Rev. **B39**, 591 (1989), and references therein.

[2] S. Chakravarty, in: "HTC: The Los Alamos Meeting", eds. K. Bedell, D. Pines and J. R. Schrieffer (in press, 1990).

[3] S. Chakravarty, B. I. Halperin, and D. Nelson, Phys. Rev. **B39**, 2344 (1989).

[4] S. Tyč, B. I. Halperin, and S. Chakravarty, Phys. Rev. Lett. **62**, 835 (1989).

[5] G. Reiter, private communication.

[6] H.-Q. Ding and M. S. Makivić, Jan. 1990 preprint.

[7] A. P. Young, Bull. Am. Phys. Soc. **34**, 896 (1989); J. D. Reger and A. P. Young, Phys. Rev **B37**, 5978 (1988).

[8] N. D. Mermin and H. Wagner, Phys. Rev. Lett. **17**, 1133 (1966).

[9] S. Tyč and B. I. Halperin, Nov. 1989, preprint.

[10] T. Becher and G. Reiter, Phys. Rev. Lett. **63**, 1004 (1989).

[11] S. H. Shenker and J. Tobochnik, Phys. Rev. **B22**, 4462 (1980).

[12] A similar product of Lorentzians appears in the dynamic structure function for the 1-D XY model, as in Eq. (3.2) of D. R. Nelson and D. S. Fisher, Phys. Rev. **B16**, 4945 (1977).

[13] C. Kawabata and A. R. Bishop, Solid State Commun. **42**, 595 (1982); ibid, **60**, 169 (1986).

[14] B. I. Halperin and P. C. Hohenberg, Phys. Rev. Lett **19**, 700 (1967).

[15] A. Auerbach and D. Arovas, Phys. Rev. Lett. **61**, 617, (1988).

Figure Captions

Fig. 1 An Ornstein-Zernicke plot, from data obtained in the Monte Carlo simulation using a 100x100 lattice. The curves are labeled by values of temperature, T/JS^2. The slope as $q^2 \to 0$ is the square of the correlation length.

Fig. 2 Estimates of the correlation length vs. T (in units of JS^2), obtained via Fig. 1 (circles), compared with the low temperature RG prediction, Eq. (2.4), using $B_\xi = 0.01$ (solid curve). At low temperature, finite size effects severely limit the correlation length obtained this way. At high temperature, the RG prediction underestimates ξ; the MC results agree with high temperature series.

Fig. 3 Typical $S(\mathbf{q},\omega)$ data and curve fits, for $\mathbf{q} = (0.1, 0.1)\pi/a$, at temperatures $T/JS^2 = 0.65$ and 0.85. The frequency is in units of $JS^2/\hbar$. The data were generated in the MC-MD calculation described in the text. The dotted curve is a least squares fit to a *product* of Lorentzians (Eq. (2.18)), using spinwave parameters shown. The dashed curve is a least squares fit to a *sum* of Lorentzians (Eq. (2.19)), for comparison (parameters not shown).

Fig. 4 More $S(\mathbf{q},\omega)$ data and curve fits, for $\mathbf{q} = (0.16, 0.16)\pi/a$, at temperatures $T/JS^2 = 0.65$ and 0.85; as described in Figure 3 caption.

Fig. 5 Spinwave frequencies $\omega_\mathbf{q}$ vs. temperature T, obtained from least squares fits as in Figures 3 and 4. The curves are labeled by wavevectors in units of $\pi/50a$. The solid curves represent the dispersion used by THC, Eq. (4.3), with parameter $\delta = 2.5$, used together with Eq. (2.4) for ξ.

Fig. 6 Spinwave frequencies $\omega_\mathbf{q}$ vs. q, obtained from least squares fits as in Figures 3 and 4. The MC-MD data are compared with the zero temperature dispersion (dashed curve, Eq. 4.2), and the dispersion used by THC, (solid curves, Eq. 4.3, with $\delta = 2.5$).

Fig. 7 The spinwave linewidth $\gamma_\mathbf{q}$ vs. q, for various temperatures T/JS^2, as indicated. Solid curves are the THC assumption, Eq. (4.4), with parameters $\gamma_0 = 1.7, \mu = 1.7$, and $\theta = 0.7$. The parameters were chosen such that the curves fit well for lower temperatures, but it was difficult to simultaneously fit the higher temperatures.

Fig. 8 The spinwave linewidth $\gamma_\mathbf{q}$ vs. temperature, for selected wavevectors, indicated in

units of $\pi/50a$. The $\mathbf{q} = (0,0)$ data is used to give preliminary estimates of the scaling frequency, ω_s.

Fig. 9 Scaled spinwave frequencies, $\omega_{\mathbf{q}}/\omega_s$ as a function of $q\xi$, using data derived at temperatures $T/JS^2 = 0.62$ (@), 0.65 (+), 0.70 (*), 0.75 (o), and 0.85 (x). Values of ω_s for each temperature, given in Table 1, were first estimated from the $q = 0$ linewidths in Fig. 8, and then corrected slightly such that the scaled frequencies from different temperatures fall on the same curve.

Fig. 10 Scaled spinwave linewidths $\gamma_{\mathbf{q}}/\omega_s$ as a function of $q\xi$, using data derived at temperatures $T/JS^2 = 0.62$ (@), 0.65 (+), 0.70 (*), 0.75 (o), and 0.85 (x). Values of ω_s used to scale the linewidths are the same as in Fig. 9.

Fig. 11 Examples of scaling the raw data for the dynamic structure function in amplitude, frequency and wavevector, as indicated, for scaled wavevectors $Q = 2.25$, 4.8, 6.1 and 11.

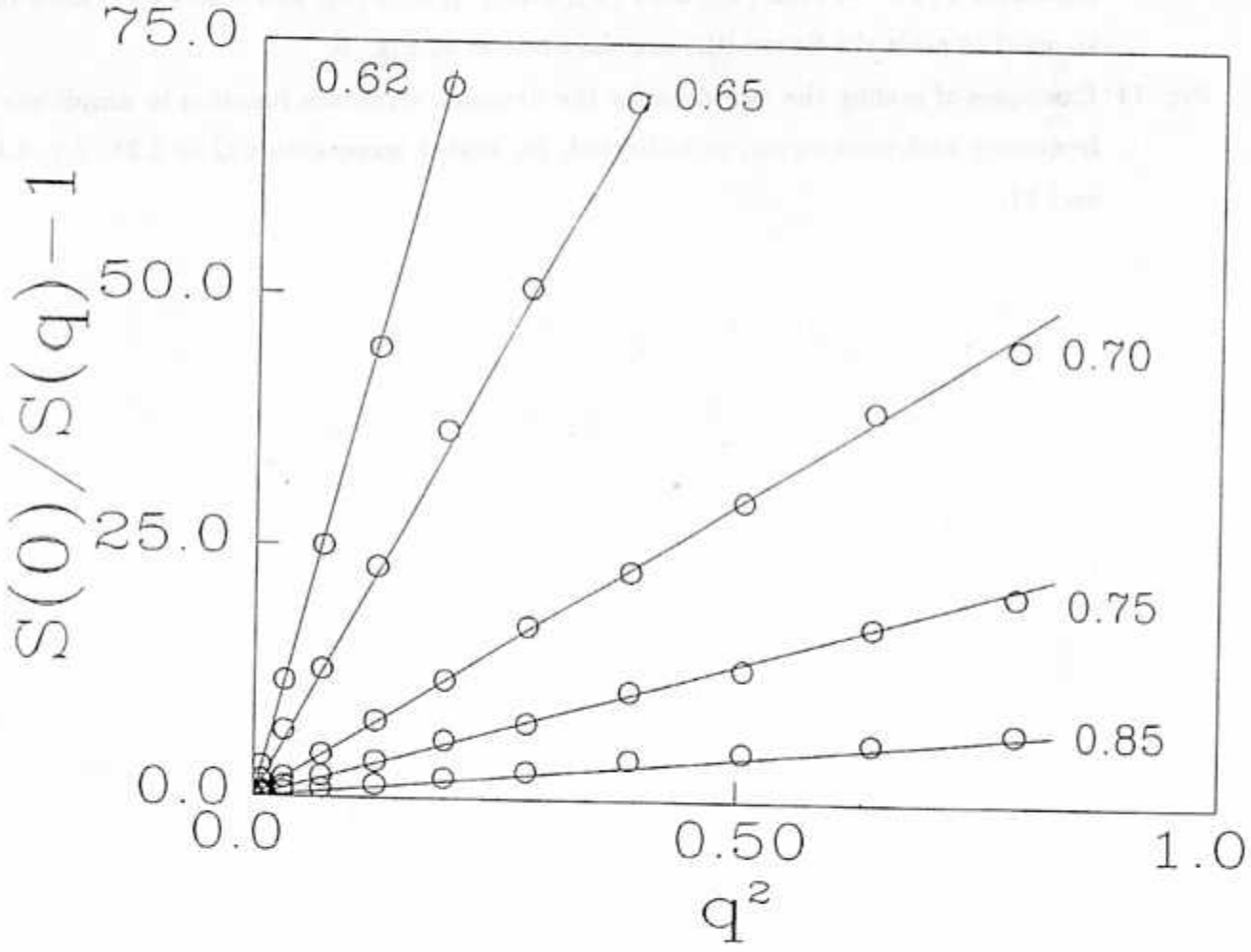

Fig. 1

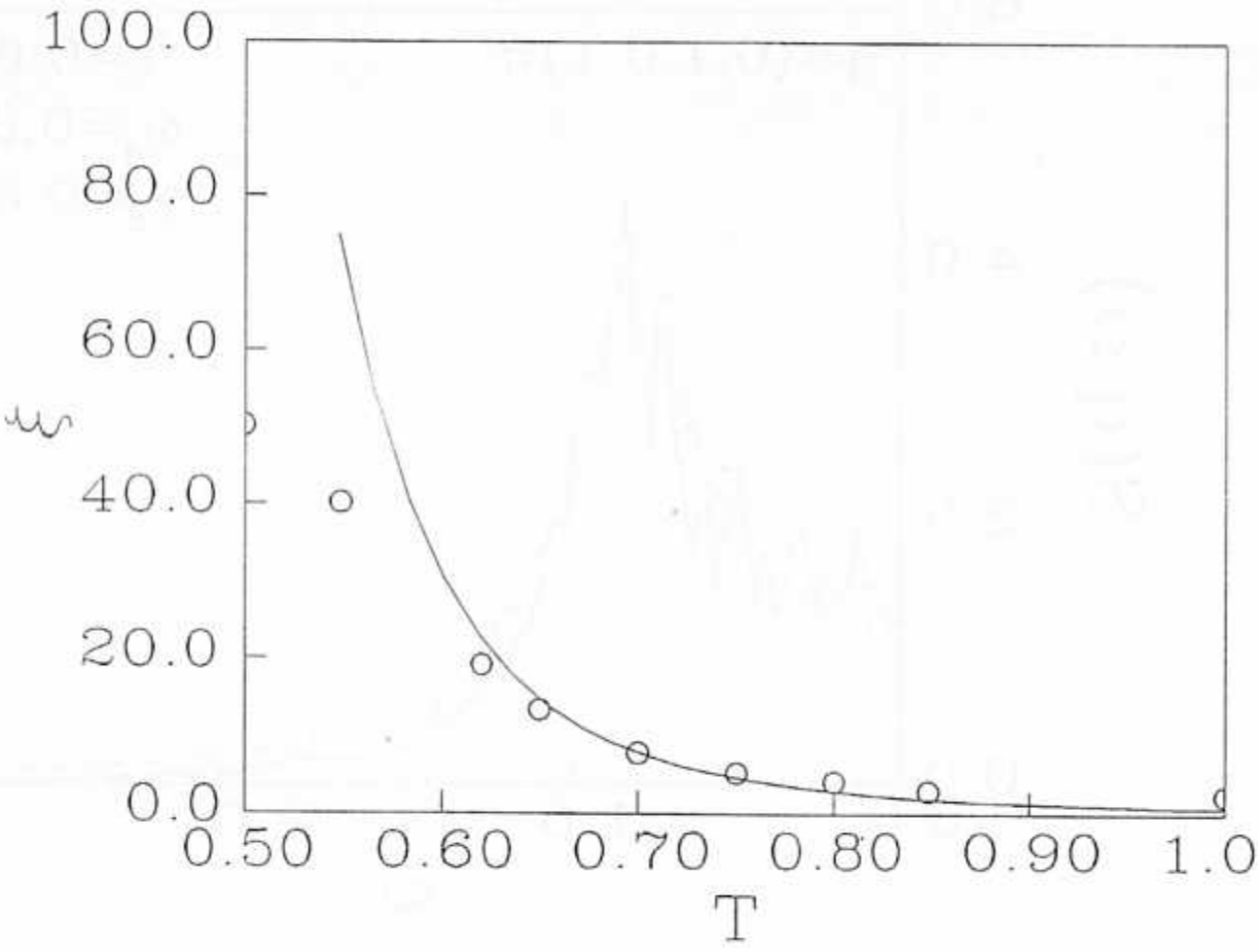

Fig. 2

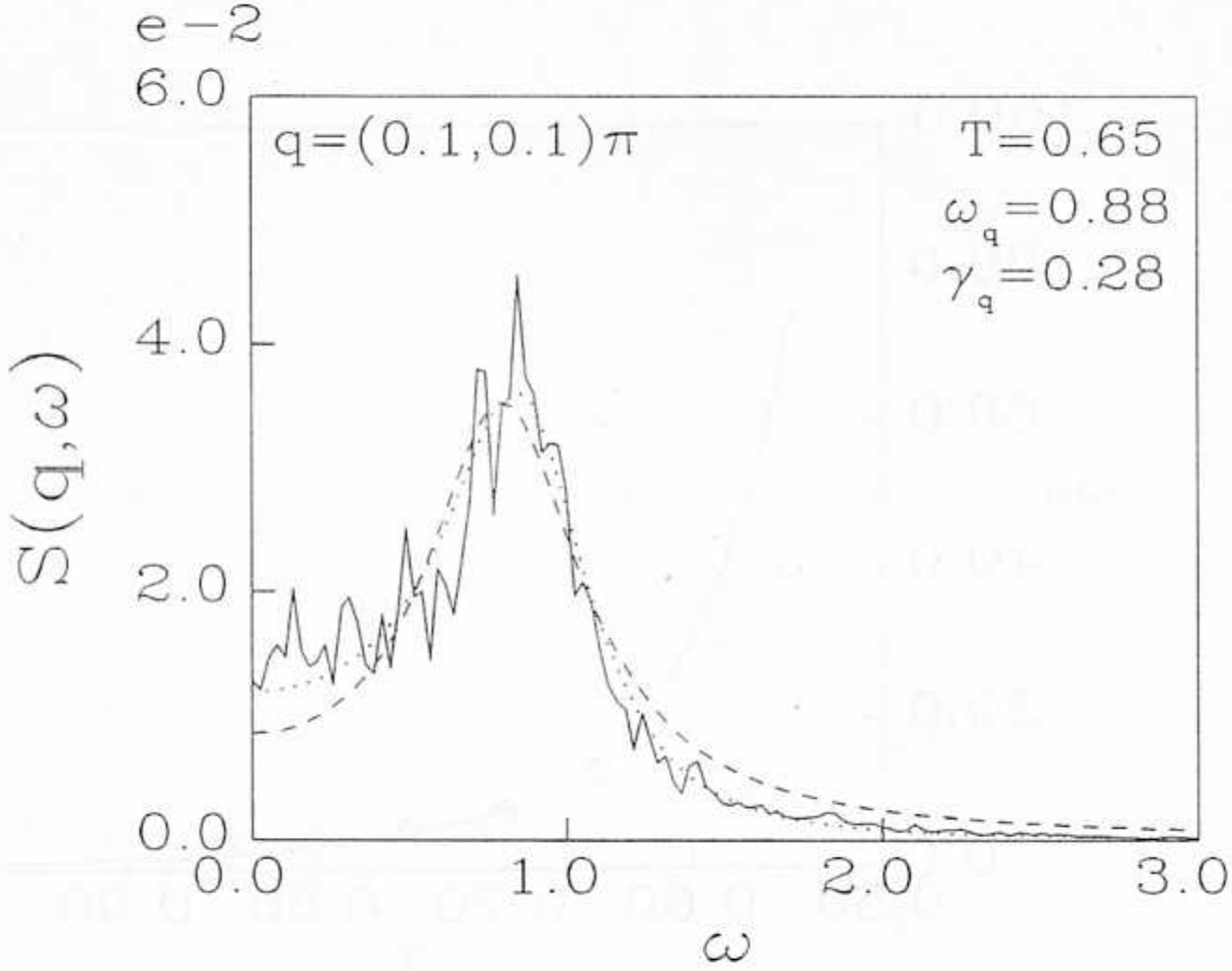

Fig 3a.

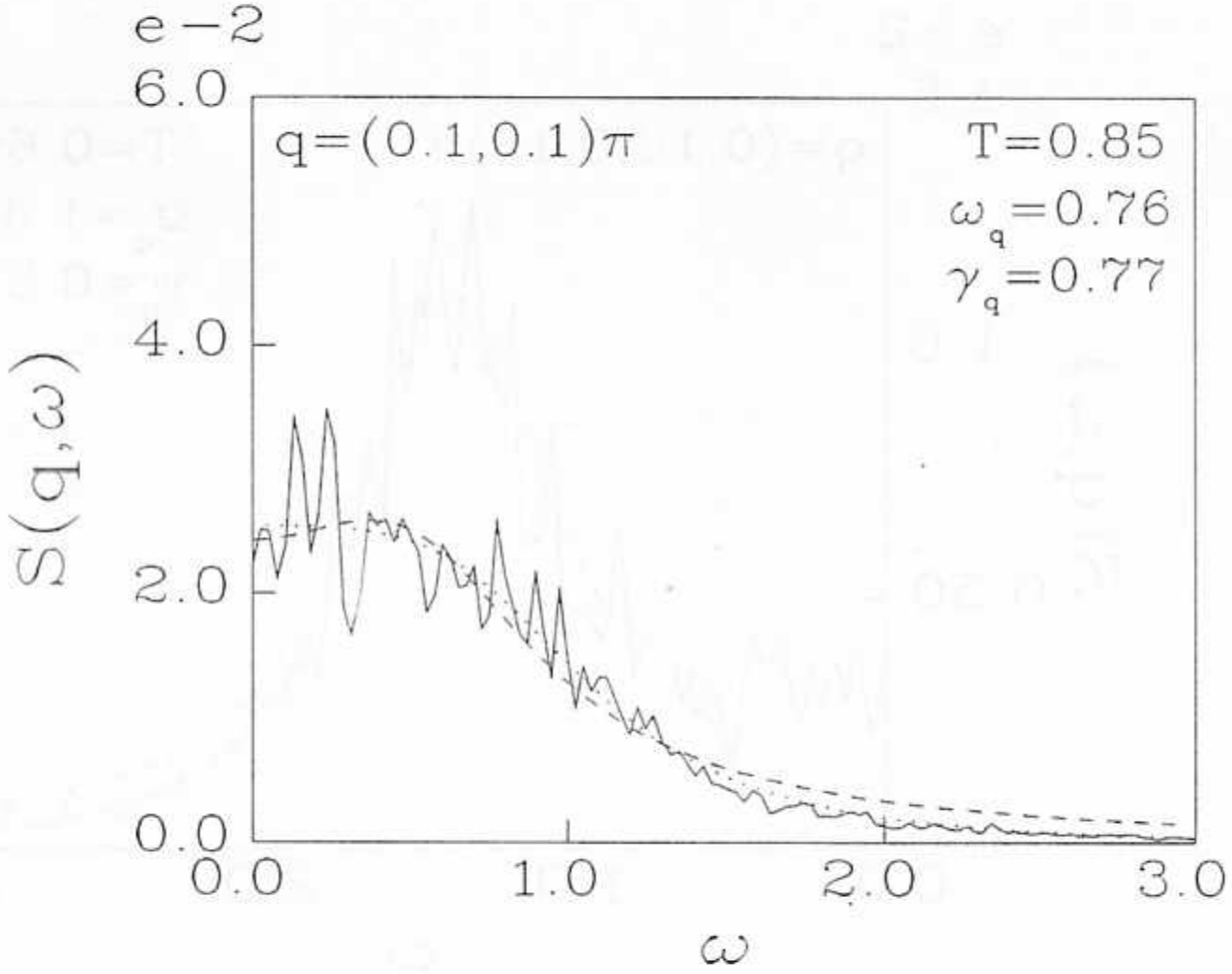

Fig 3b

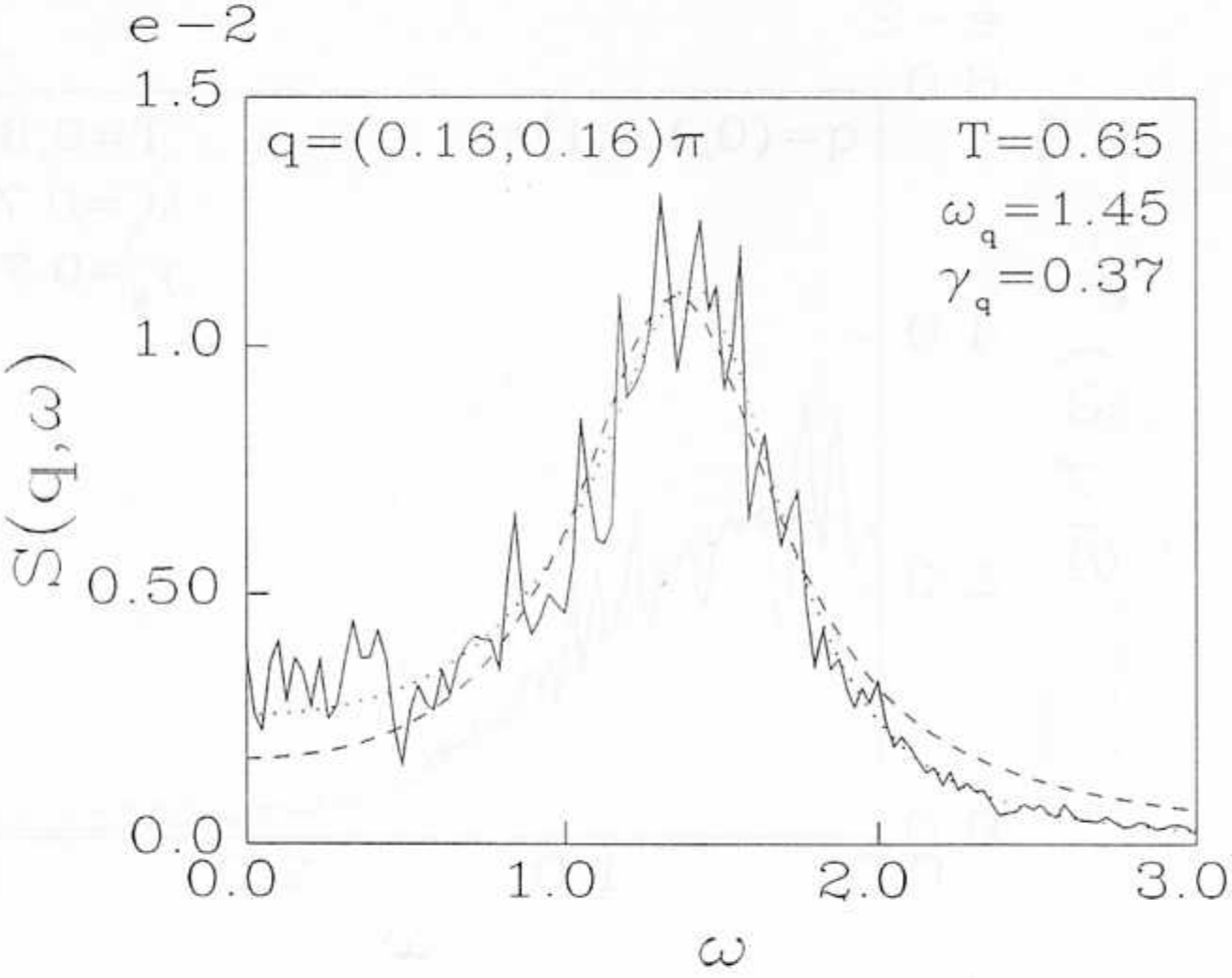

Fig 4a.

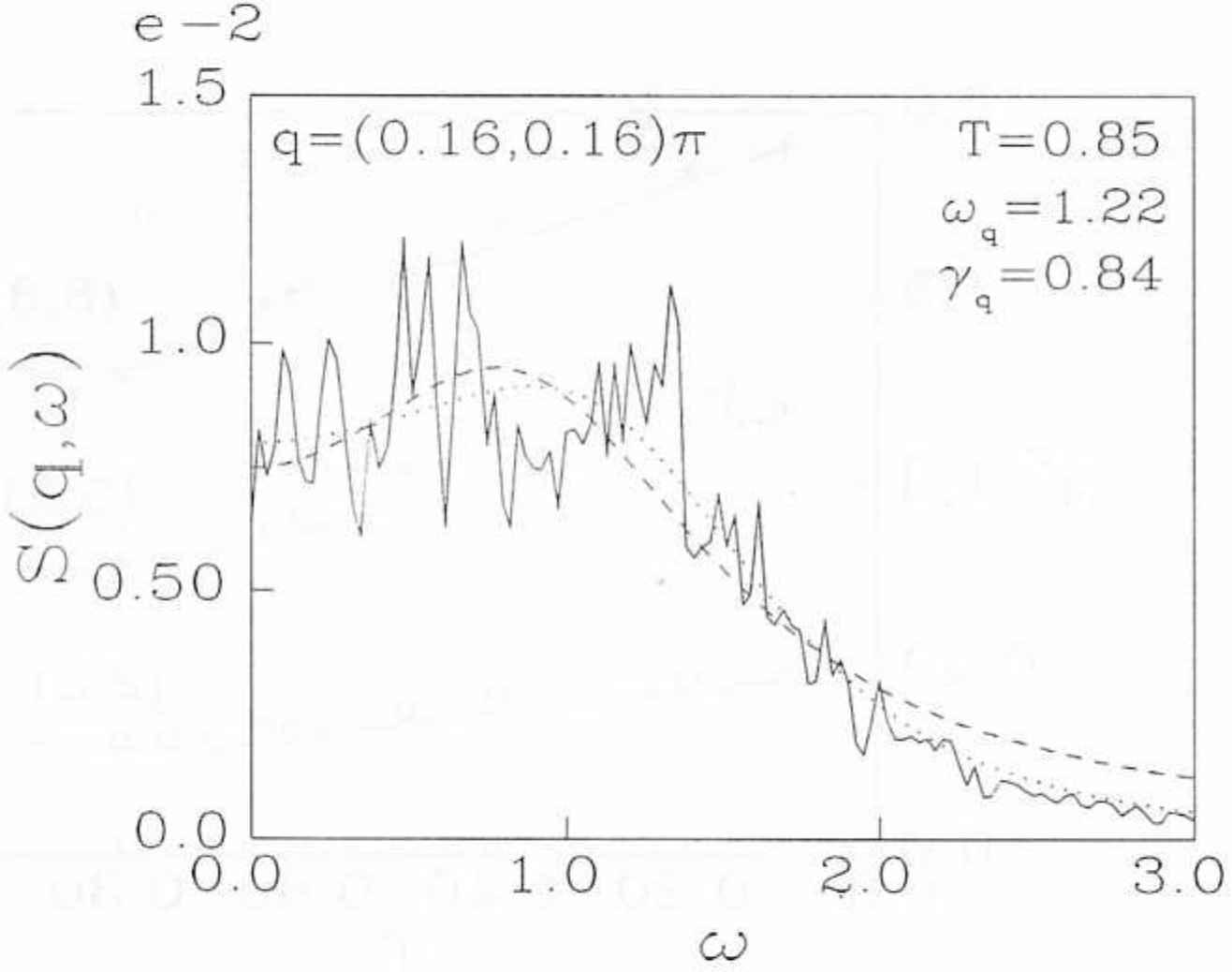

Fig 4b

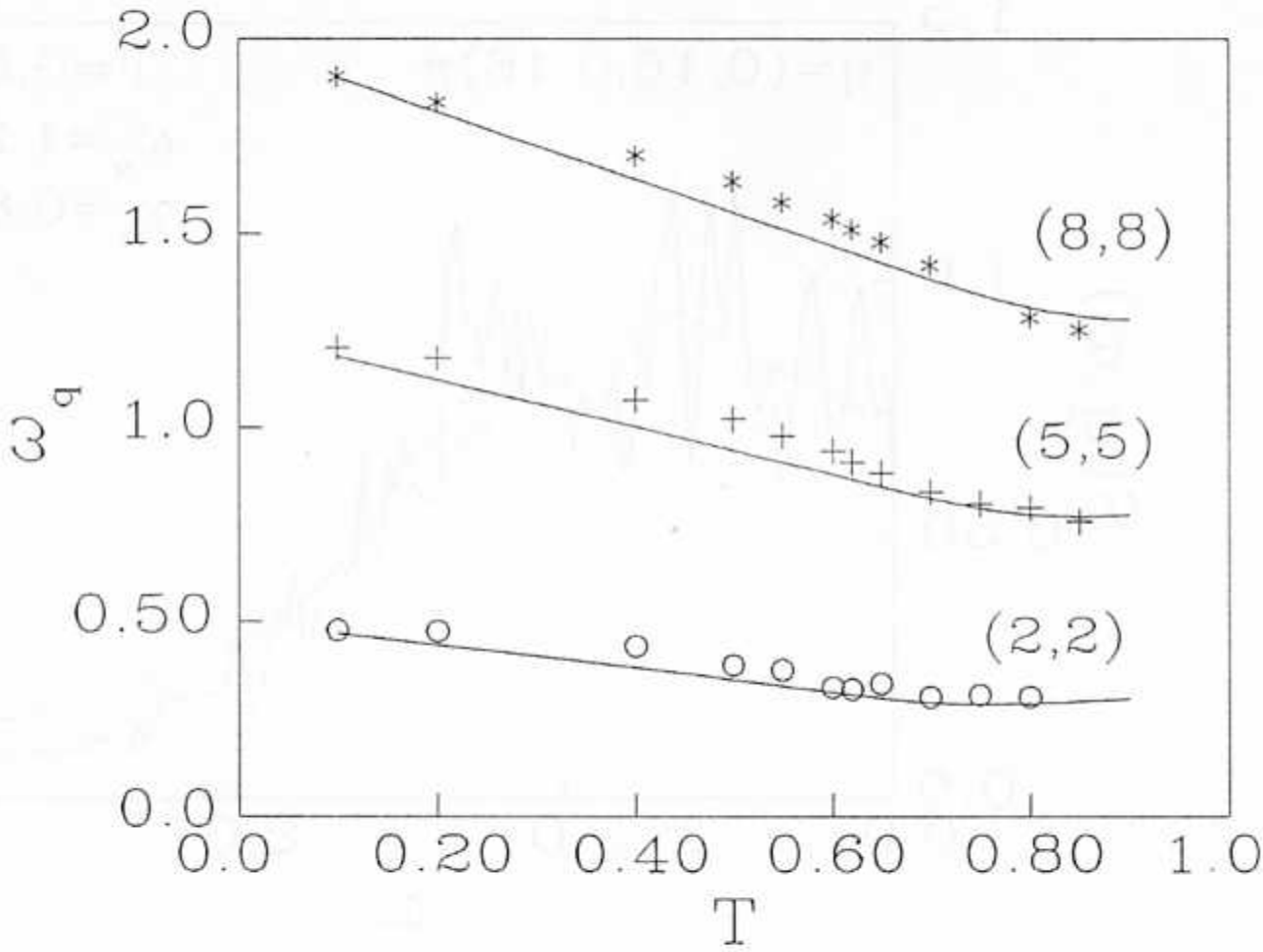

Fig 5

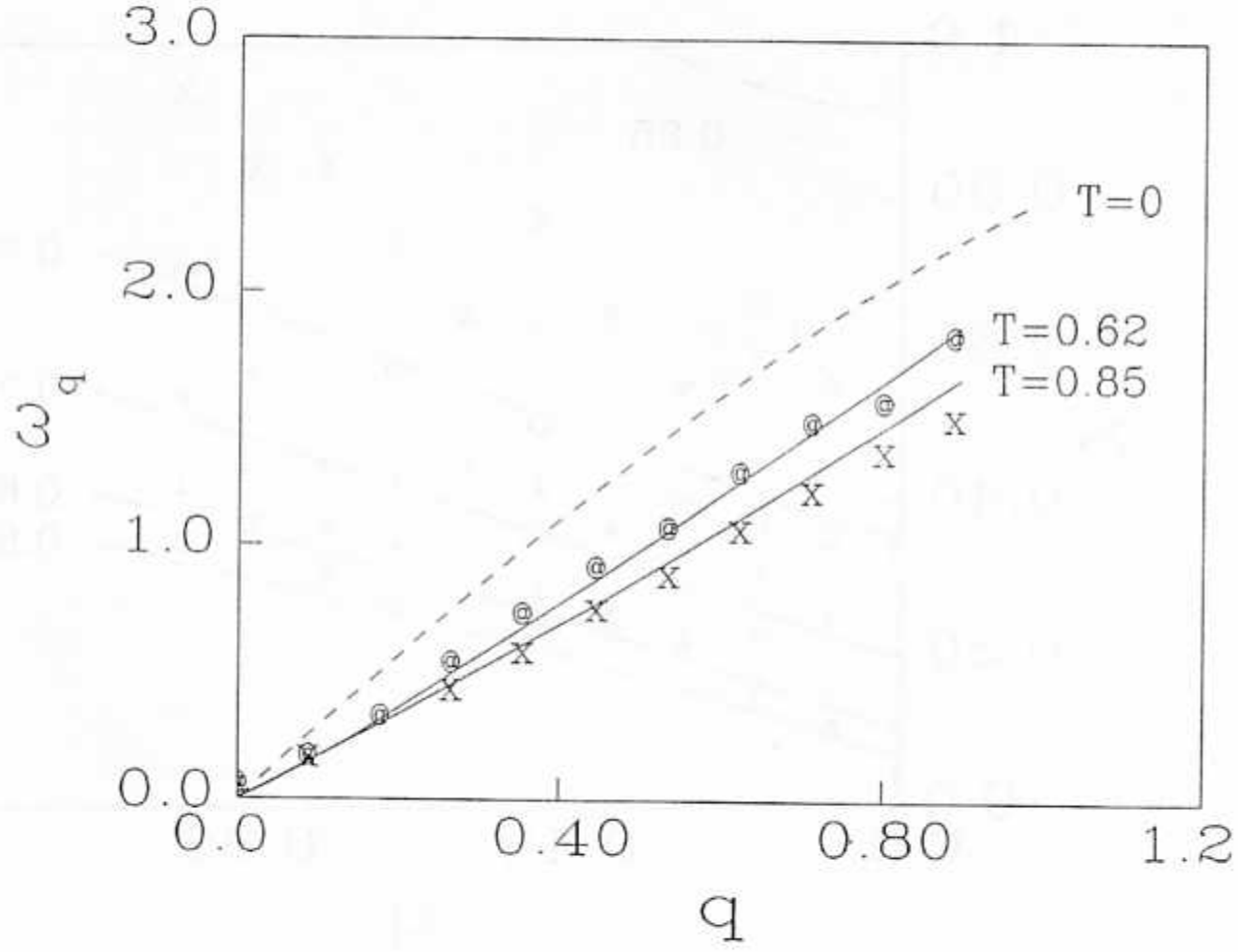

Fig 6.

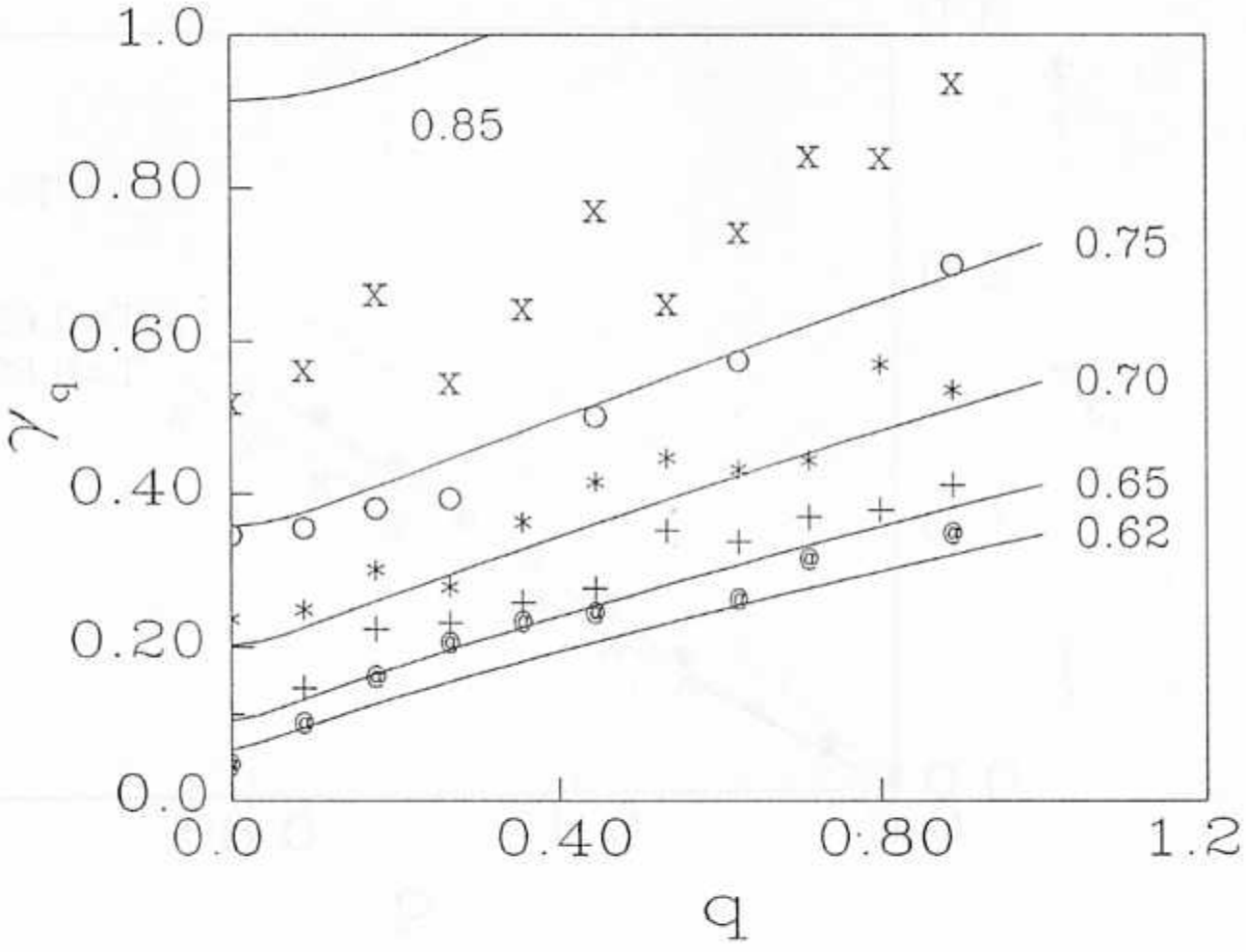

Fig 7.

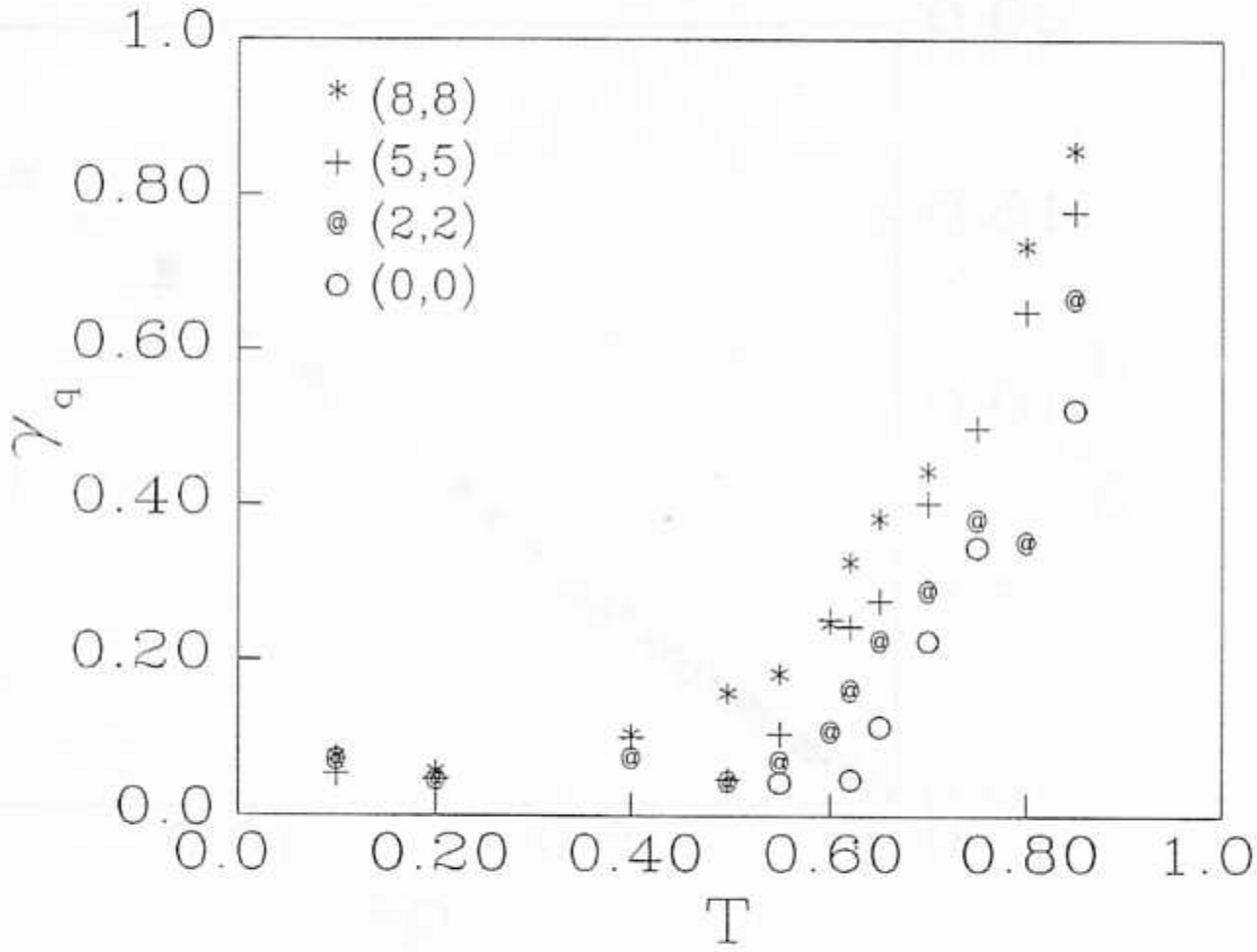

Fig 8.

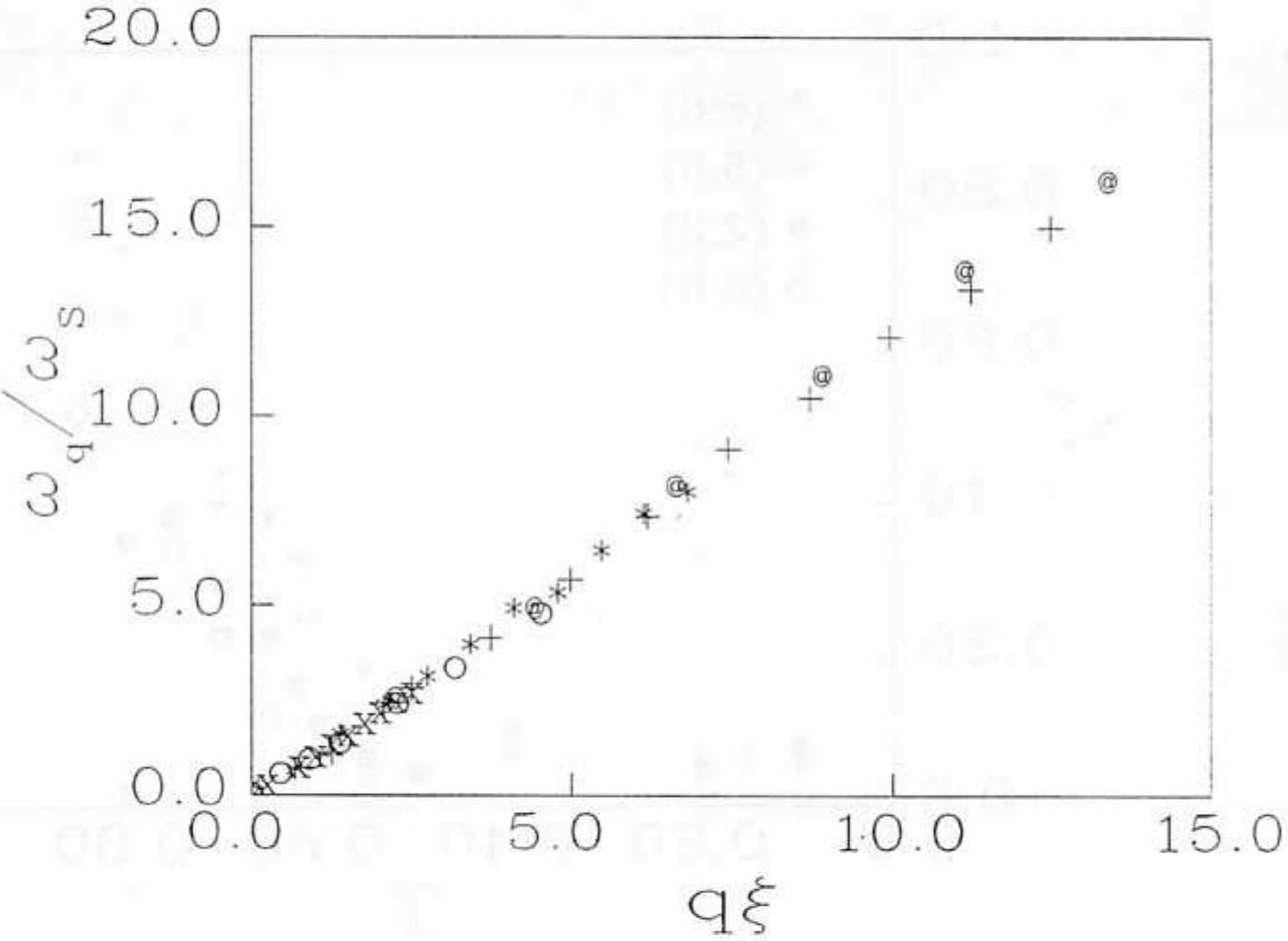

Fig 9.

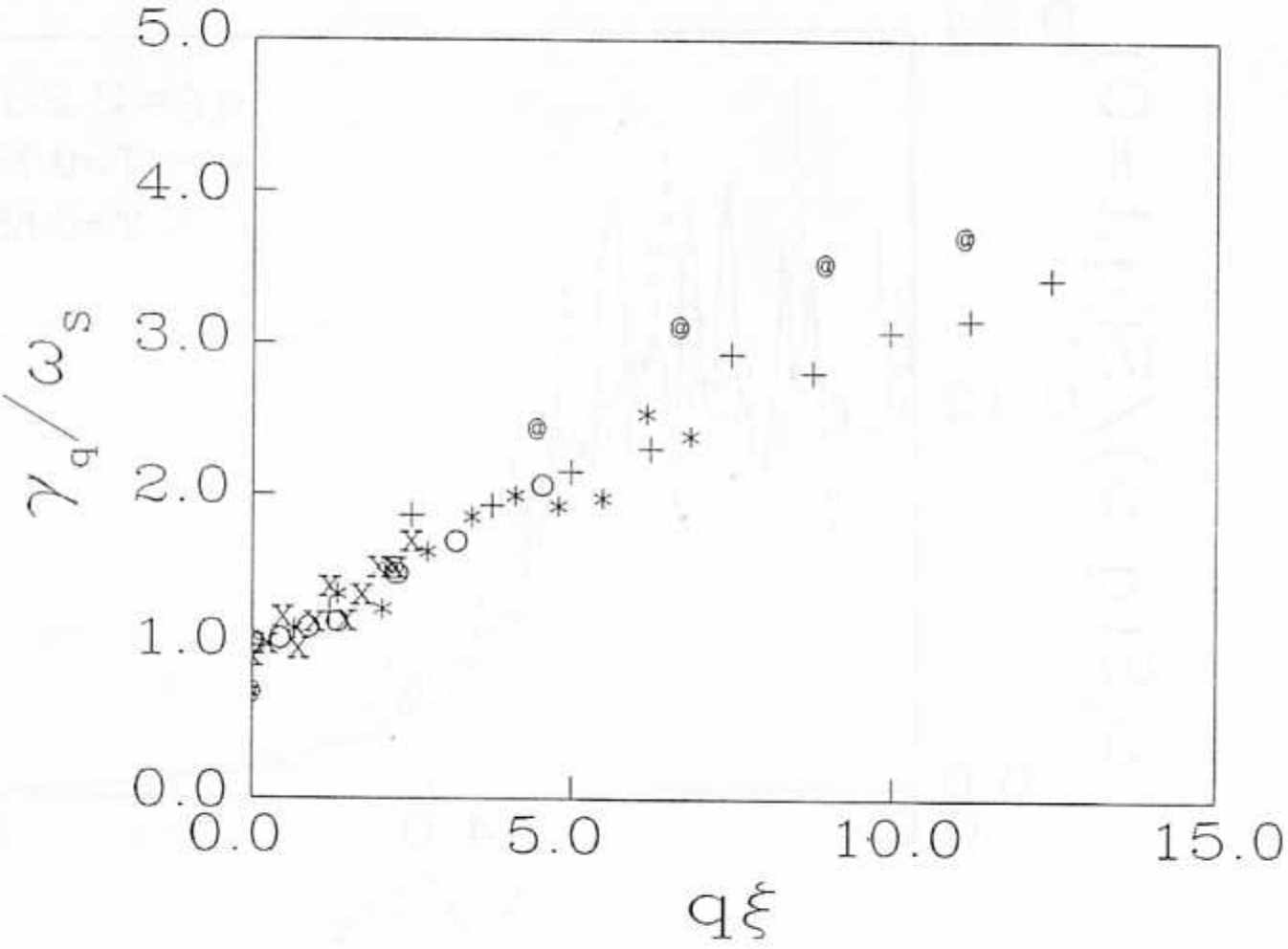

Fig 10.

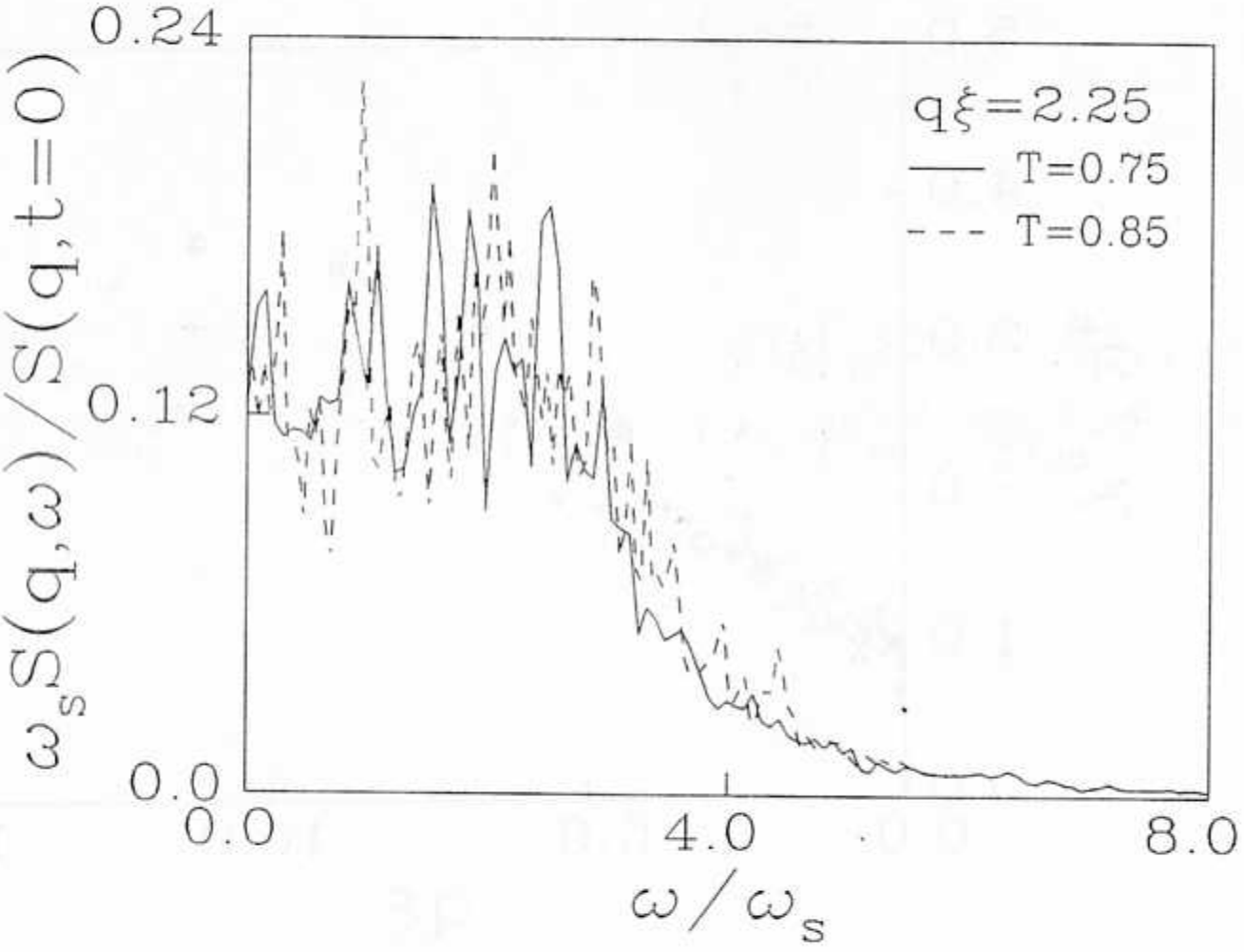
0.24
0.12
0.0
0.0
4.0
8.0
$\omega_s S(q,\omega)/S(q,t=0)$
ω/ω_s
$q\xi=2.25$
T=0.75
T=0.85

Fig 11a.

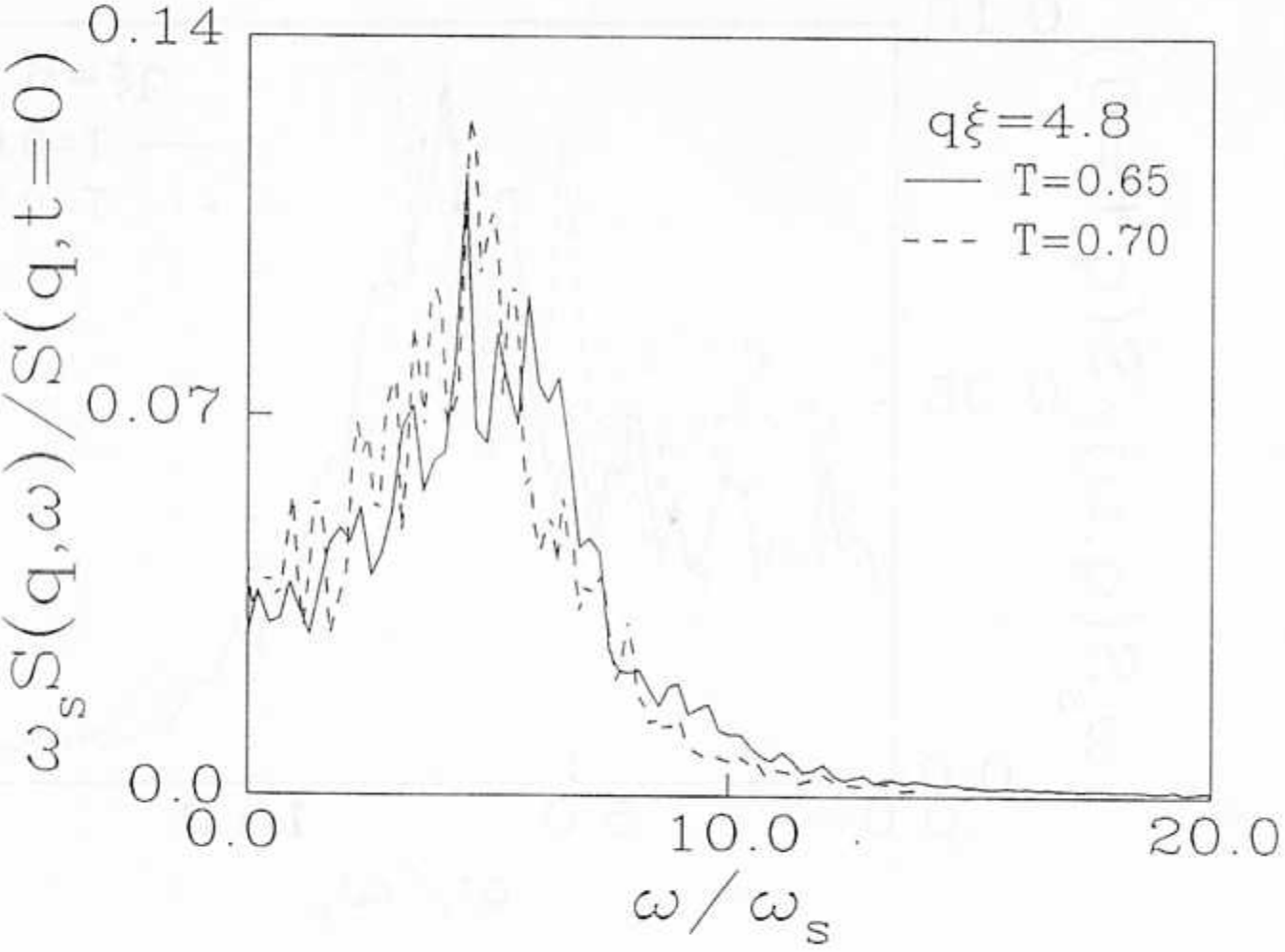
0.14
0.07
0.0
0.0
10.0
20.0
$\omega_s S(q,\omega)/S(q,t=0)$
ω/ω_s
$q\xi=4.8$
T=0.65
T=0.70

Fig 11b

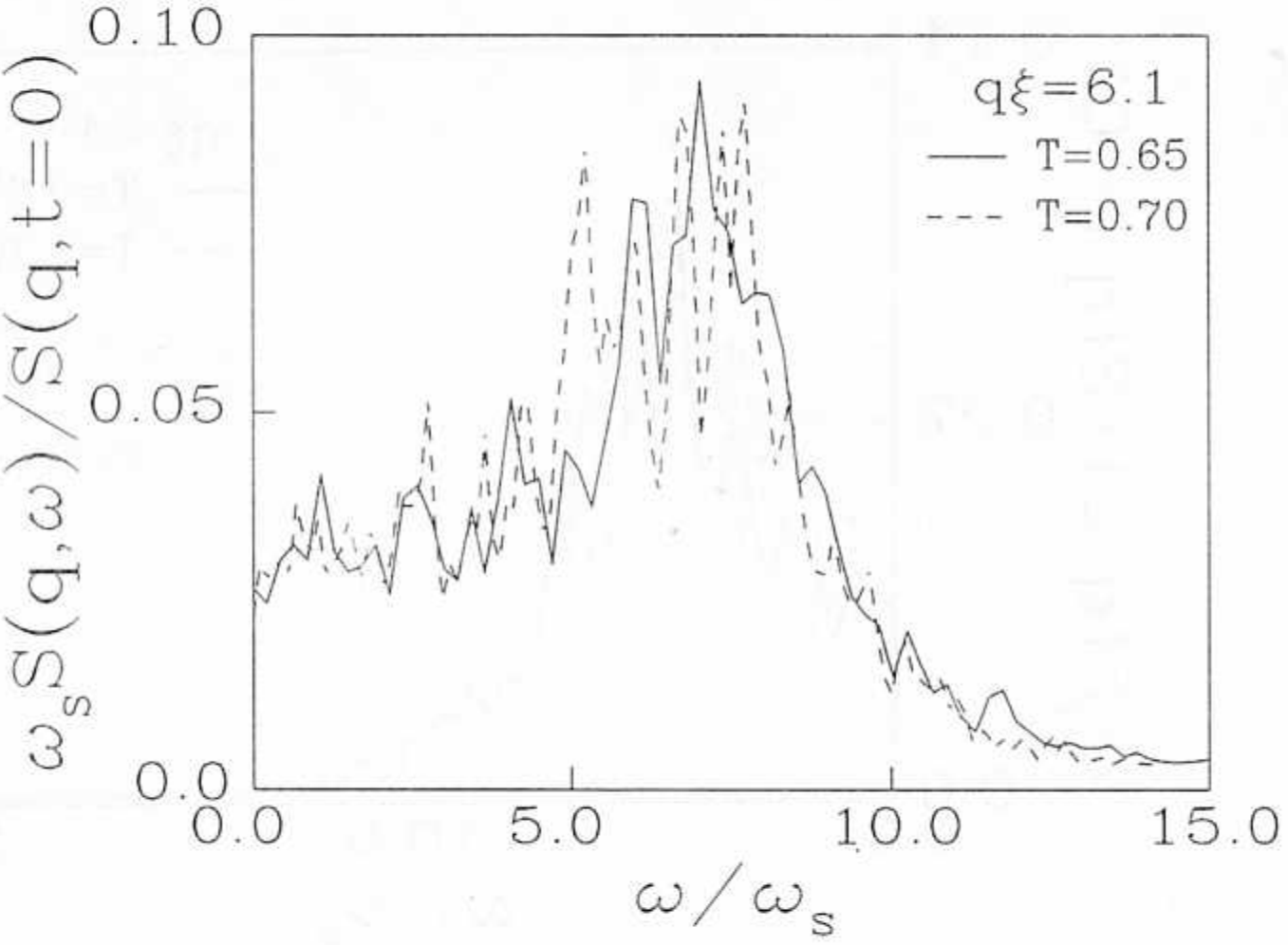
0.10
0.05
0.0
0.0
5.0
10.0
15.0
$\omega_s S(q,\omega)/S(q,t=0)$
ω/ω_s
$q\xi=6.1$
T=0.65
T=0.70

Fig IIc.

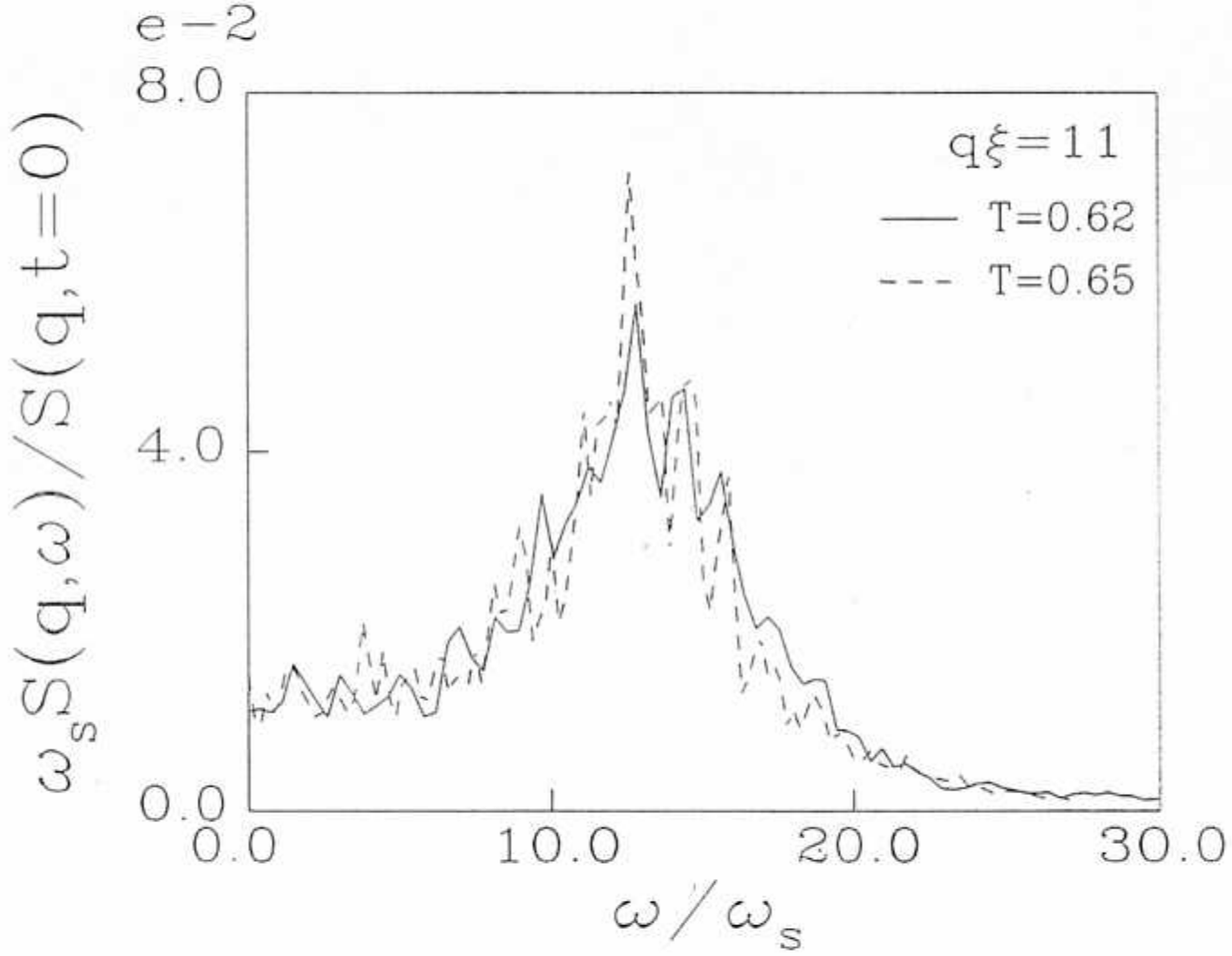
e−2
8.0
4.0
0.0
0.0
10.0
20.0
30.0
$\omega_s S(q,\omega)/S(q,t=0)$
ω/ω_s
$q\xi=11$
T=0.62
T=0.65

Fig. 11d.